INVITED PAPER

Toward Robotic Sensor Webs: Algorithms, Systems, and Experiments

Recent advances in wireless sensor networks and collections of stationary and mobile sensors including robots are reviewed in this paper, which also presents novel ideas on system architecture and design.

By Hoam Chung, *Member IEEE*, Songhwai Oh, *Member IEEE*, David Hyunchul Shim, *Member IEEE*, and S. Shankar Sastry, *Fellow IEEE*

ABSTRACT | This paper presents recent advances in multiagent sensing and operation in dynamic environments. Technology trends point towards a fusion of wireless sensor networks with robotic swarms of mobile robots. In this paper, we discuss the coordination and collaboration between networked robotic systems, featuring algorithms for cooperative operations such as unmanned aerial vehicles (UAVs) swarming. We have developed cooperative actions of groups of agents such as probabilistic pursuit-evasion game for search and rescue operations, protection of resources, and security applications. We have demonstrated a hierarchical system architecture which provides wide-range sensing capabilities to unmanned vehicles through spatially deployed wireless sensor networks, highlighting the potential collaboration between wireless sensor networks and unmanned vehicles. This paper also includes a short review of our current research efforts in heterogeneous sensor networks, which is being evolved into mobile sensor networks with swarm mobility. In a very essential way, this represents the fusion of mobility of ensembles with the network embedded systems, the robotic sensor web.

KEYWORDS | Heterogeneous wireless sensor network; multiagent cooperation; robotic swarms

I. INTRODUCTION

The distributed control of multiple autonomous agents has become a very important research topic since individual agents were rapidly connected to each other through various communication mediums. Although a centralized system can be implemented using a simpler structure than a distributed system, the latter is preferred since a multiagent system is more robust against local faults and free from communication bottlenecks. Without a central coordinator, however, achieving basic properties such as stability, coordination, and coverage offers serious challenges, and there have been many proposals and implementations to control and manage such a system; see [1]–[5], for example.

A wireless sensor network (WSN) is a relatively new addition to multiagent systems research. A WSN consists of a large number of spatially distributed devices with computing and sensing capabilities, i.e., motes, which form an *ad hoc* wireless network for communication [6]–[8]. Applications of WSNs include, but are not limited to, building energy management [9], environmental monitoring [10], traffic control [11], manufacturing [12], health services [13], indoor

Manuscript received May 10, 2010; revised February 19, 2011; accepted May 7, 2011. Date of publication July 14, 2011; date of current version August 19, 2011. This work was supported by many U.S. government agencies including ARO, AFOSR, DARPA, and ONR. Particularly, this paper is directly supported by ARO MURI Scalable sWarms of Autonomous Robots and Mobile Sensors (W911NF-0510219), Heterogeneous Sensor Webs for Automated Target Recognition and Tracking in Urban Terrain (W911NF-06-1-0076), and ARL Micro Autonomous Systems and Technology Collaborative Technology Alliance (MAST-CTA, W91INF-08-2-0004). The work of H. Chung was supported in part by Monash Engineering New Staff Research Grants. The work of S. Oh was supported in part by the Basic Science Research Program through the National Research Foundation of Korea (NRF) funded by the Ministry of Education, Science and Technology (2010-0013354). The work of D. H. Shim was supported in part by Korea Agency for Defense Development Grant ADDR-401-101761.
H. Chung is with the Department of Mechanical and Aerospace Engineering, Monash University, Clayton, Vic. 3800, Australia (e-mail: hoam.chung@monash.edu).
S. Oh is with the School of Electrical Engineering and Computer Science and the Automation and Systems Research Institute (ASRI), Seoul National University, Seoul 151-744, Korea (e-mail: songhwai@snu.ac.kr).
D. H. Shim is with the Department of Aerospace Engineering, Korea Advanced Institute of Science and Technology, Daejon 305-701, Korea (e-mail: hcshim@kaist.ac.kr).
S. S. Sastry is with the Department of Electrical Engineering and Computer Science, University of California Berkeley, Berkeley, CA 94720 USA (e-mail: sastry@eecs.berkeley.edu).

Digital Object Identifier: 10.1109/JPROC.2011.2158598

 0018-9219/$26.00 ©2011 IEEE

localization [14], and surveillance [15]. Until mid 2000s, the research was focused on the development of devices [16], [17], wireless communication protocols [18], and distributed inference algorithms [19], [20], for stationary sensor nodes. Thanks to the recent advances in microelectromechanical systems (MEMS) technology, distributed time synchronization [21], and ultralow-power processors [22], a sensor node can have more sensors even on a smaller form factor than before while consuming less power. The most exciting feature now being added to the traditional WSN research is the mobility. Biologically inspired microrobots are now being developed [23]–[28], and these will provide the ability to move around environments for active sensing.

This trend creates a new junction where the WSN technologies meet the distributed control of autonomous mobile agents, which we call the robotic sensor web (RSW) in this paper. The cooperative robotic sensor nodes will provide better sensing coverage with a smaller number of nodes than stationary sensors while more adaptively responding to operator commands. However, the RSW implemented on microrobots or miniature robots offers a new set of challenges. Given the limitations in size, weight, and power of small robots, it is understood that individual platforms will be less capable than larger robots. Computation, communication, and power are coupled with each other but available onboard resources will be severely limited. As a result, it is envisioned that the cooperation between robotic sensor nodes of multiple scales and types will be required to achieve mission objectives.

In the Robotics and Intelligent Machines Laboratory at the University of California Berkeley (UC Berkeley), we have been working on the operations of autonomous agents and the various research topics in WSNs.

BEkeley AeRobot (BEAR) team was established in 1996 in the laboratory. The team developed fundamental technologies for rotorcraft-based unmanned aerial vehicles (UAVs), and achieved its first autonomous hovering in 1999 [29]. Following the success, a Yamaha R50 helicopter was automated, and a basic waypoint navigation interface was implemented [30]. The first cooperative behavior between an autonomous UAV and multiple unmanned ground vehicles (UGVs) was demonstrated in the probabilistic pursuit-evasion game setup [31], and showed that the global-max policy outperforms the local-max policy in capturing an evader. In early 2000s, multiple Yamaha helicopters were automated [32], and they were used in the formation flight experiments, in which two real and seven virtual helicopters were used [33]. In the following years, the team has been focusing on multivehicle coordination and conflict resolution scheme based on model-predictive control (MPC) algorithms [34]–[38].

Our work in wireless sensor networks was initiated by the participation in the network embedded systems technology (NEST) project funded by the Defense Advanced Research Projects Agency (DARPA). Our WSN research group has produced many theoretical and technological breakthroughs in wireless sensor networks and networked control systems, which include the distributed control within wireless networks [39], estimation with intermittent observations [40], and tracking and coordination using WSNs [41]. In the last few years, we have been working on heterogeneous sensor networks (HSNs), which are composed of wireless sensors with various sensing capabilities and communication bandwidths.

Two groups are now jointly working on the RSWs, and have been participating in Micro Autonomous Systems and Technology Collaborative Technology Alliance (MAST-CTA) [42] since 2008.

In this paper, we first summarize our previous results in tracking and coordination of multiple agents using WSNs, and recent progress in HSNs. In Section IV, algorithms for coordinated control of UAV swarms using the MPC approach are presented. As our concluding remarks, we present a short review of ongoing research in RSWs.

II. WIRELESS SENSOR NETWORKS

Multitarget tracking and a pursuit evasion game (PEG) were demonstrated at the DARPA NEST final experiment on August 30, 2005. In this section, we summarize experimental results reported in [41].

The experiment was performed on a large-scale, long-term, outdoor sensor network testbed deployed on a short grass field at UC Berkeley's Richmond Field Station (see Fig. 1). A total of 557 sensor nodes were deployed and 144 of these nodes were allotted for the tracking and PEG experiments. However, six out of the 144 nodes used in the experiment were not functioning on the day of the demo, reflecting the difficulties of deploying large-scale, outdoor systems. The sensor nodes were deployed at approximately 4–6 m spacing in a 12 × 12 grid. Each sensor node was elevated using a camera tripod to prevent the passive

(a) (b)

Fig. 1. ***Hardware for the sensor nodes. (a) Trio sensor node on a tripod. On top is the microphone, buzzer, solar panel, and user and reset buttons. On the sides are the windows for the passive infrared sensors. (b) A live picture from the two-target PEG experiment.***

infrared (PIR) sensors from being obstructed by grass and uneven terrain [see Fig. 1(a)]. The true locations of the nodes were measured during deployment using differential global positioning system (GPS) and stored in a table at the base station for reference. However, in the experiments the system assumed the nodes were placed exactly on a 5-m spacing grid to highlight the robustness of the system against localization error.

In order to solve the multitarget tracking and pursuit evasion game, we have proposed a hierarchical real-time control system *LochNess* which is shown in Fig. 2. *LochNess* is composed of seven layers: the sensor networks, the multisensor fusion (MSF) module, the multitarget tracking (MTT) modules, the multitrack fusion (MTF) module, the multiagent coordination (MAC) module, the path planner module, and the path follower modules.

Under this architecture, sensors are spread over the surveillance region and form an *ad hoc* network. The sensor network detects moving objects in the surveillance region and the MSF module converts the sensor measurements into target position estimates (or reports) using spatial correlation. We consider a hierarchical sensor network. In addition to regular sensor nodes ("Tier-1" nodes), we assume the availability of "Tier-2" nodes which have long-distance wireless links and more processing power. We assume that each Tier-2 node can communicate with its neighboring Tier-2 nodes. Examples of a Tier-2 node include high-bandwidth sensor nodes such as iMote and BTnode [43], gateway nodes such as Stargate, Intrinsyc Cerfcube, and PC104 [43], and the Tier-2 nodes designed for our experiment [16]. Each Tier-1 node is assigned to its nearest Tier-2 node and the Tier-1 nodes are grouped by Tier-2 nodes. We call the group of sensor nodes formed around a Tier-2 node a "tracking group." When a node detects a possible target, it listens to its neighbors for their measurements and fuses the measurements to forward to its Tier-2 node. Each Tier-2 node receives the fused measurements from its tracking group and the MTT module in each Tier-2 node estimates the number of evaders, the positions and velocities of the evaders, and the estimation error bounds. Each Tier-2 node communicates with its neighboring Tier-2 nodes when a target moves away from the region monitored by its tracking group. Last, the tracks estimated by the Tier-2 nodes are combined hierarchically by the MTF module at the base station.

The estimates computed by the MTF module are then used by the MAC module to estimate the expected capture

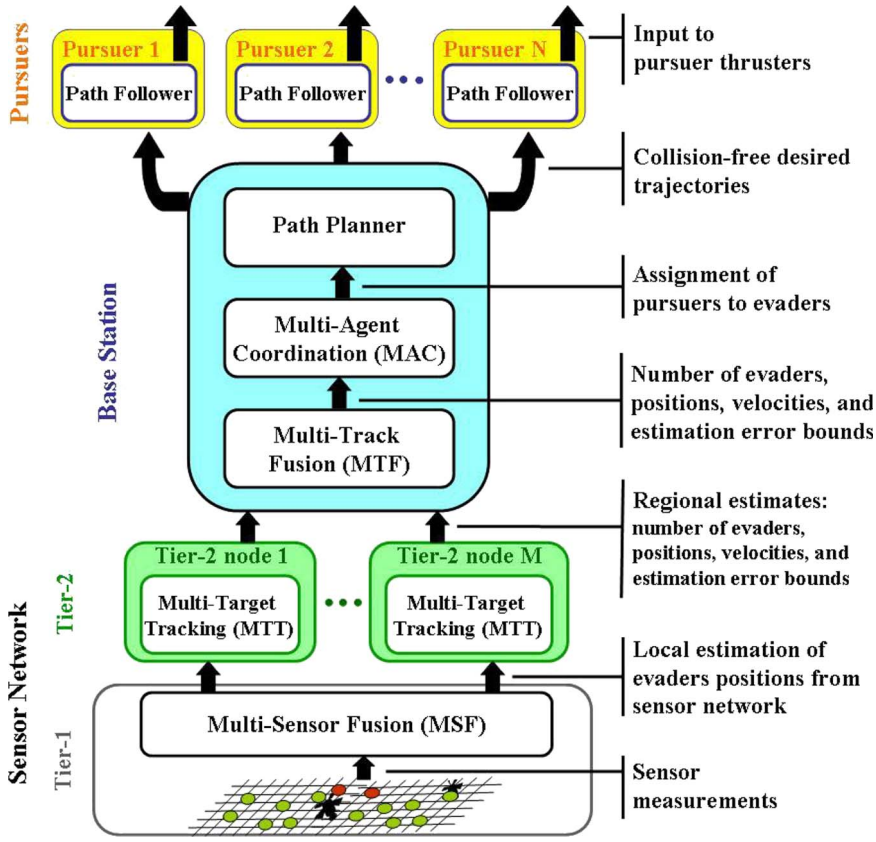

Fig. 2. ***LochNess: a hierarchical real-time control system architecture using wireless sensor networks for multitarget tracking and multiagent coordination.***

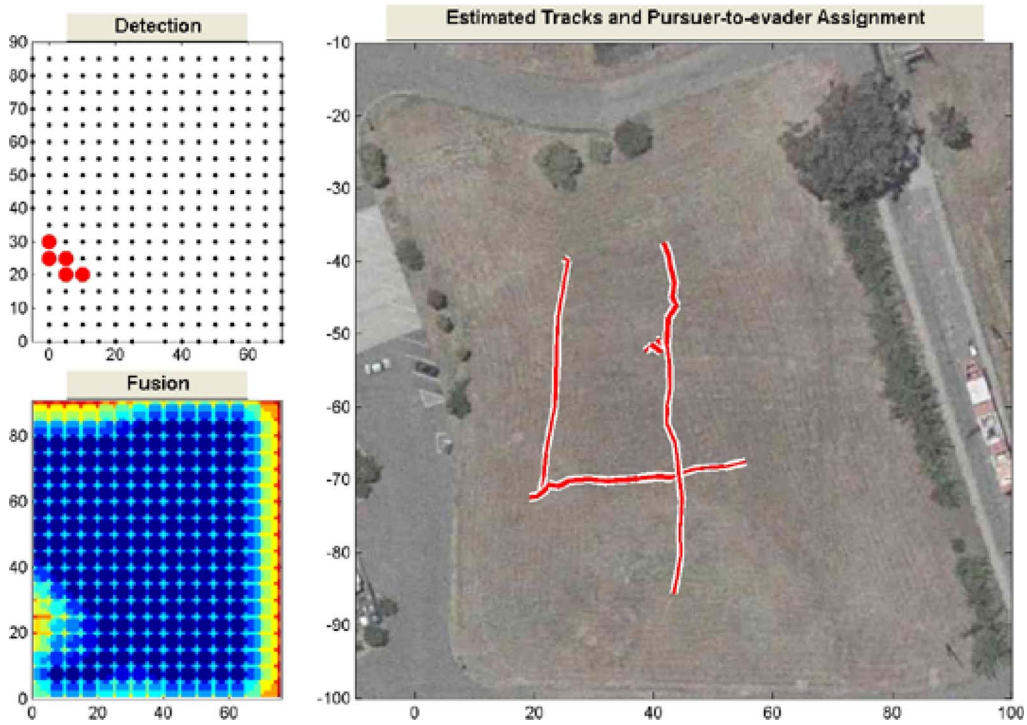

Fig. 3. ***Estimated tracks of targets at time 70 from the experiment with three people walking in the field. (Upper left) Detection panel. Sensors are marked by small dots and detections are shown in large disks. (Lower left) Fusion panel shows the fused likelihood. (Right) Estimated tracks and pursuer-to-evader assignment panel shows the tracks estimated by the MTT module, estimated evader positions (stars) and pursuer positions (squares). See Fig. 4.***

times of all pursuer–evader pairs. Based on these estimates, the MAC module assigns one pursuer to one evader by solving the bottleneck assignment problem [44] such that the estimated time to capture the last evader is minimized. Once the assignments are determined, the path planner module computes a trajectory for each pursuer to capture its assigned evader in the least amount of time without colliding into other pursuers. Then, the base station transmits each trajectory to the path-following controller of the corresponding pursuer. The path-following controller modifies the pursuer's trajectory on the fly to avoid any obstacles sensed by the pursuer's onboard sensors. For the MTT and MTF modules, we used the online multiscan Markov chain Monte Carlo data association (MCMCDA) algorithm [45] for solving multi-target tracking and multitrack fusion problems. It has been shown that MCMCDA is a fully polynomial randomized approximation scheme for a single-scan Bayesian data association problem and MCMCDA approximates the optimal Bayesian filter when applied to the multiscan data association problems [45]. For more detail about the description about the system used in the experiments, see [41].

We demonstrated the system on one, two, and three human targets, with targets entering the field at different times. In all three experiments, the tracking algorithm correctly estimated the number of targets and produced correct tracks. Furthermore, the algorithm correctly disambiguated crossing targets in the two-target and three-target experiments without classification labels on the targets. Fig. 3 shows the multitarget tracking results with three targets walking through the field. The three targets entered and exited the field around time 10 and 80, respectively. During the experiment, the algorithm correctly rejected false alarms and compensated for missing detections. There were many false alarms during the span of the experiments. Though not shown in the figures, the algorithm dynamically corrected previous track hypotheses as it received more sensor readings.

In another demonstration, two simulated pursuers were dispatched to chase two crossing human targets. The pursuer-to-target assignment and the robust minimum time-to-capture control law were computed in real time, in tandem with the real-time tracking of the targets. The simulated pursuers captured the human targets, as shown in Fig. 4. In particular, note that the MTT module is able to correctly disambiguate the presence of two targets [right panel of Fig. 4(a)] using past measurements, despite the fact that the multisensor fusion (MSF) module reports the detection of a single target [upper left panel of Fig. 4(a)]. A live picture of this experiment is shown on the right of Fig. 1.

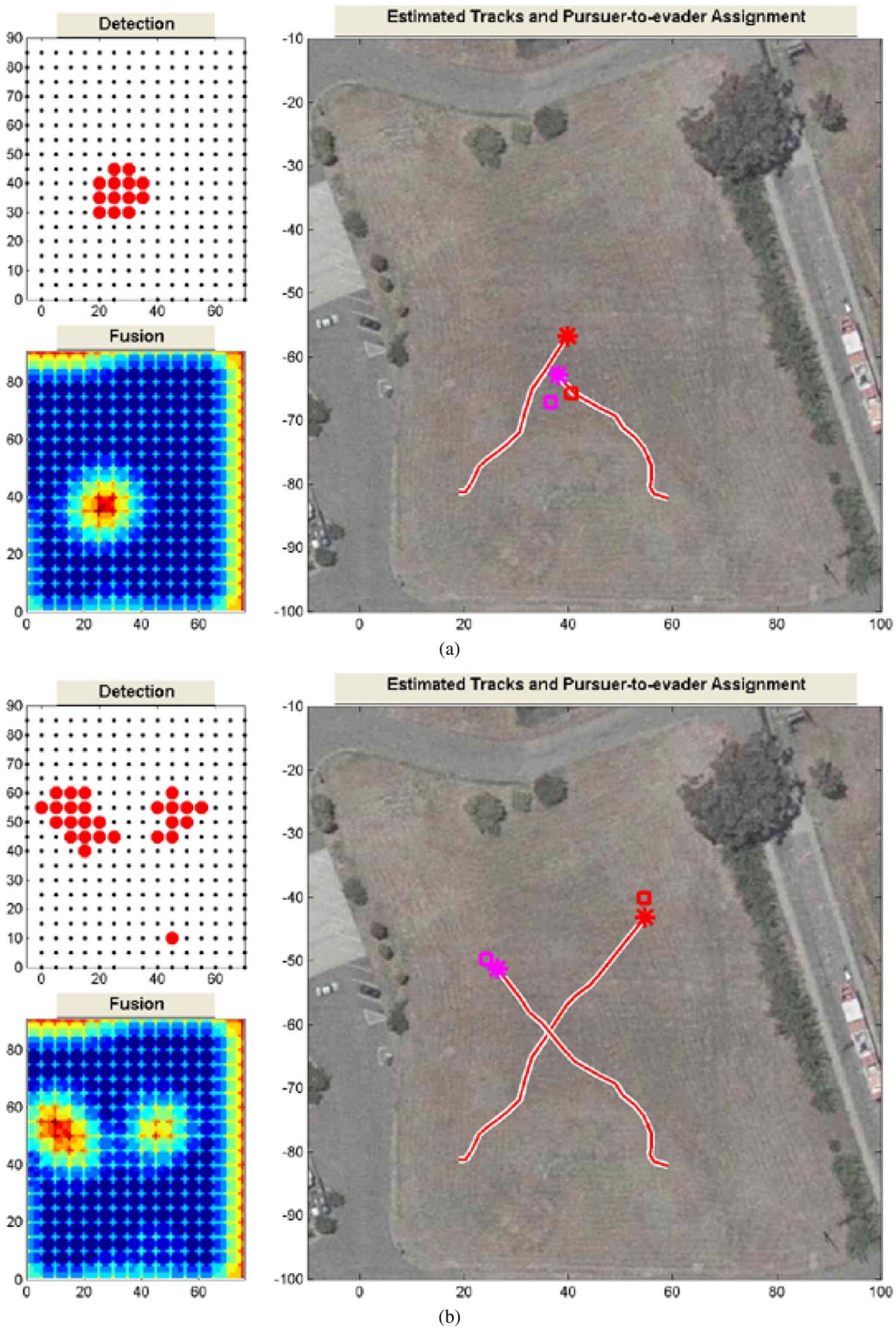

Fig. 4. ***Estimated tracks of evaders and pursuer positions from the pursuit evasion game experiment. (a) Before crossing. (b) After crossing.***

III. HETEROGENEOUS SENSOR NETWORKS

The research in WSNs has traditionally focused on low-bandwidth sensors (e.g., acoustic, vibration, and infrared sensors) that limit the ability to identify complex, high-level physical phenomena. This limitation can be addressed by integrating high-bandwidth sensors, such as

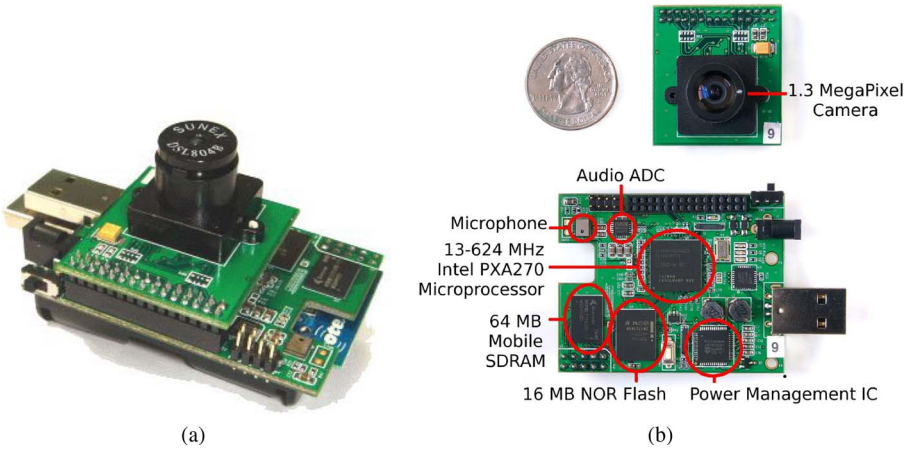

Fig. 5. ***(a) A CITRIC camera mote. (b) A camera daughter board with major functional units outlined.***

image sensors, to provide visual verification, in-depth situational awareness, recognition, and other capabilities. This new class of WSNs is called heterogeneous sensor networks (HSNs). The integration of high-bandwidth sensors and low-power wireless communication in HSNs requires new in-network information processing techniques and networking techniques to reduce the communication cost for long-term deployment. The best example of HSNs is a camera sensor network [46]. Camera sensor networks (e.g., CITRIC motes [46]; see Fig. 5) can address the limitations of low-bandwidth sensors by providing visual verification, in-depth situational awareness, recognition, and other capabilities. The CITRIC mote is a wireless camera hardware platform with a 1.3 megapixel camera, a PDA class processor, 64-MB RAM, and 16-MB FLASH.

CITRIC motes form a wireless network and they must operate in an uncontrolled environment without human intervention. In order to fully take advantage of the information from the network, it is important to know the position of the cameras in the network as well as the orientation of their fields of view, i.e., *localization*. By localizing the cameras, we can perform better in-network image processing, scene analysis, data fusion, power handoff, and surveillance. While there are localization methods for camera networks, they all make artificial requirements. For example, in [47], a common set of static scene feature points is assumed to be seen by each set of three cameras. In [48], the height of the cameras is already known as well as two orientation parameters. In [20] and [49], a single object is tracked in a common ground plane and it is already known how each camera locally maps to the ground plane. This ground plane concept is extended in [50] and [51] but the localization problem is solved by using the track of a single object.

We removed these artificial requirements and developed a camera network localization method that can be used even when cameras are wide-baseline[1] or have different photometric properties [52]. The method is also applied to recover the orientations and positions of the CITRIC motes [46]. The method can reliably compute the orientation of a camera's view and position *only* up to a scaling factor. We removed this restriction by combining our technique with radio interferometry [53] to recover the exact orientation and position in [54].

A. Localization Algorithm Overview

We make no prior assumptions on where the cameras are placed except that there must be some field-of-view overlap between pairs of cameras if the orientation, up to a scaling factor, and position of those cameras are to be recovered. Furthermore, we do not make any assumptions on known correspondences or about the scene structure. For example, the cameras may be wide baseline and no prior knowledge of how each camera's coordinate frame is related to the ground of the scene is known.

By observing moving objects in the scene, we localize the cameras. Our procedure consists of three main steps in order to use individual raw video streams to localize the cameras: an intracamera step, an intercamera step, and then a global recovery step. The intracamera step, which we call *track formation*, involves exploiting similarities of objects between frames for each camera separately. The intercamera step, which we call *track matching*, involves using the object image tracks from each camera as features to compare against object image tracks from other cameras. The steps are as follows.

1) Track formation: Find moving objects in each camera's field of view and based on correspondences between frames, build tracks of those

[1]The line connecting the centers of a pair of cameras is called the *baseline*.

(a) (b)

Fig. 6. ***Track formation: formation of tracks based on object motion in two separate cameras. (a) Camera 1. (b) Camera 2.***

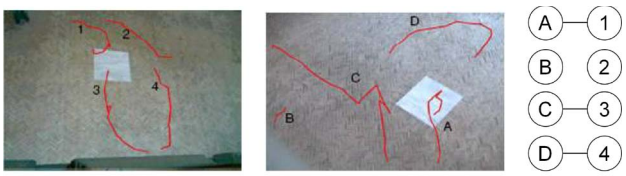

(a) (b) (c)

Fig. 7. ***Track matching: (a) shows the tracks in a single camera (b) shows the tracks from another camera over the same time period, and (c) shows the correct track matching between the two cameras that is used in the essential matrix computation.***

objects within the image plane as shown in Fig. 6. Multiscan MCMCDA [45] is used to find tracks.

2) Track matching: Use the image tracks from each camera as features to compare against image tracks from another cameras in order to determine the relative orientation and position of each camera. This comparison is done in a pairwise manner and is based on the properties of the essential matrix, which is computed using the standard algorithm [55]. This is illustrated in Fig. 7.
3) Global recovery: Transform all relative coordinates of the cameras into a global coordinate frame.

B. Experiment—Three-Camera Network

Here we show the results on data from a camera network of three cameras. Images from the network can be seen in Fig. 8. In this setup, three cameras were placed in a wide baseline configuration on a second story balcony of a building looking down at the first floor. Tracks of people walking on the first floor were used to localize the cameras. Three different sequences of 60 s of video footage were used. As we had control over the environment, ground truth for the position and orientation of the cameras was obtained using a point light source and using the EasyCal Calibration Toolbox [56].

The resulting error in the estimated position, up to a scaling factor, can be seen in Table 1 and the estimated orientation error can be seen in Table 2. The center camera's coordinate frame was chosen as the world coordinate frame and the right and left cameras aligned to the center camera's coordinate frame in the global recovery step. It can be seen that the error in the estimation of the localization parameters is small even though we used the centroids of the objects in the scene to build the image tracks and then used the estimated track points to do the correspondence.

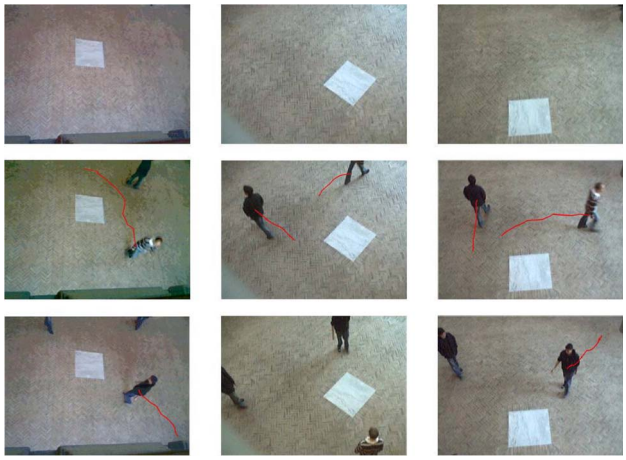

Fig. 8. ***A three-camera network. Top row: Images from the cameras with no moving objects. Middle and bottom rows: Images from cameras with tracks of moving objects shown over time.***

C. Experiment—CITRIC Camera Motes

In this experiment, we positioned two CITRIC motes 8.5 ft apart and pointed them at an open area where people were walking, as shown by the top row of pictures in Fig. 9. Each camera mote ran background subtraction on its current image and then sent the bounding box coordinates back to the base station for each detected foreground object. The center of each bounding box was used to build the image tracks over time on the base station computer, as

TABLE 1 Position Error: The Error in the Estimated Position, Up to a Scaling Factor, From the Tracks Is Given in Degrees Between Position Vectors

Camera	Sequence 1	Sequence 2	Sequence 3
Right	5.04	6.22	5.81
Left	4.11	7.68	5.91
Center	0	0	0

TABLE 2 Orientation Error: The Error in the Estimated Orientation From the Tracks Is Given in Degrees Here

Camera	Sequence 1	Sequence 2	Sequence 3
Right	1.42	3.67	2.84
Left	2.13	2.56	3.21
Center	0	0	0

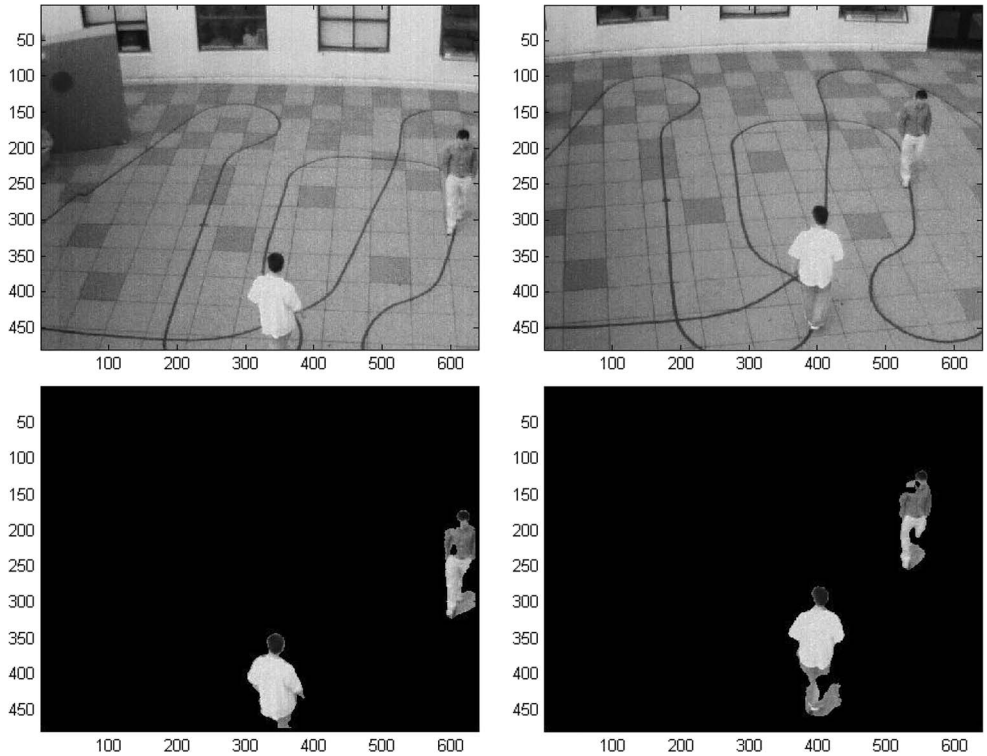

Fig. 9. ***(Top) Image frames from the left and right camera motes, respectively, viewing the scene. (Bottom) The detected foreground objects from the scene.***

shown in Fig. 10. It can be seen that multiple tracks are successfully estimated from the image sequence.

The localization algorithm then takes these tracks and performs multiple-view track correspondence. This method is particularly suitable for a low-bandwidth camera network because it works well on wide-baseline images and images lacking distinct static features [52]. Furthermore, only the coordinates of the foreground objects need to be transmitted, not entire images. In implementing the localization, tracks from the two image sequences are compared, and we adapt the method such that minimizing reprojection error determines which tracks best correspond between images. We used 43 frames from the cameras at an image resolution of 640 × 480. Foreground objects were detected in 22 of the 43 frames and tracks were built from these detected foreground objects. Four tracks were built in the first camera and five tracks were built in the second camera. We were able to determine the

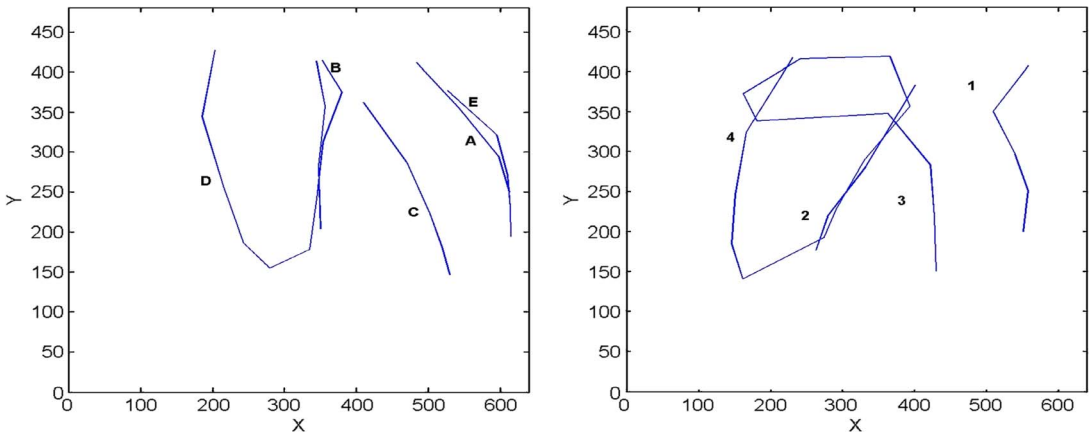

Fig. 10. ***The tracks of the moving objects in the image planes of the left and right camera motes, respectively, formed by MCMCDA.***

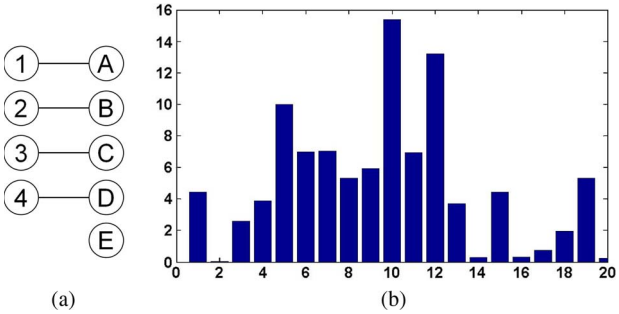

Fig. 11. ***(a) The matching of tracks between the cameras that were used for localization. (b) The reprojection error, measured in pixels, for each of the 20 points of the tracks.***

localization of the two cameras relative to one another with an average reprojection error of 4.94 pixels (see Fig. 11). This was based on the matching of four tracks between the two cameras which minimize the reprojection error.

The accuracy of the camera localization estimate is affected by a few factors. First, the choice of the (low-cost) camera has an effect on the quality of the captured image. Second, the precision of the synchronization between the cameras affects the accuracy of the image correspondence. Last, we only used a small number of frames to estimate track correspondence. Using a longer image sequence with more data points can reduce the estimation error as shown in the next section.

D. Experiment—Fusion-Based Full Localization

Using cameras only, we can recover camera positions only up to a scaling factor. In [54], we described a method for obtaining full localization, including the scaling factor, by combining the described camera network localization method and radio interferometry [53].

Our method has been tested on a real network of six cameras. We used Logitech Quick Cam Pro 4000 cameras and XSM motes [57]. We had a network of six camera nodes with 7 XSM motes. The ground truth location of the cameras+XSM motes is shown in Fig. 12. The cameras had a resolution of 240 × 320 pixels and acquired images at 8 frames per second (fps). Twelve minutes of data were taken from the cameras and used for localization. Multiple types of objects moved through the scene during this recording. Objects include a robot, a plane, a person, and a box followed by a person.

We ran adaptive background subtraction on the images from each camera and obtained the foreground objects. We built bounding boxes around the objects and if the bounding box of the object was at the edge of the image, we did not use those detections of foreground objects. Using the remaining centroids, we built object image tracks. We assumed that tracks need to be at least 4 s long to further constrain the tracks we use. This meant that at our frame rate there are at least 32 data points in a track. Tracks detected by the algorithm are shown in Fig. 13. We used the tracks for feature correspondence between the cameras and solved for orientations and positions of all cameras. Fig. 14 shows what cameras are visually connected

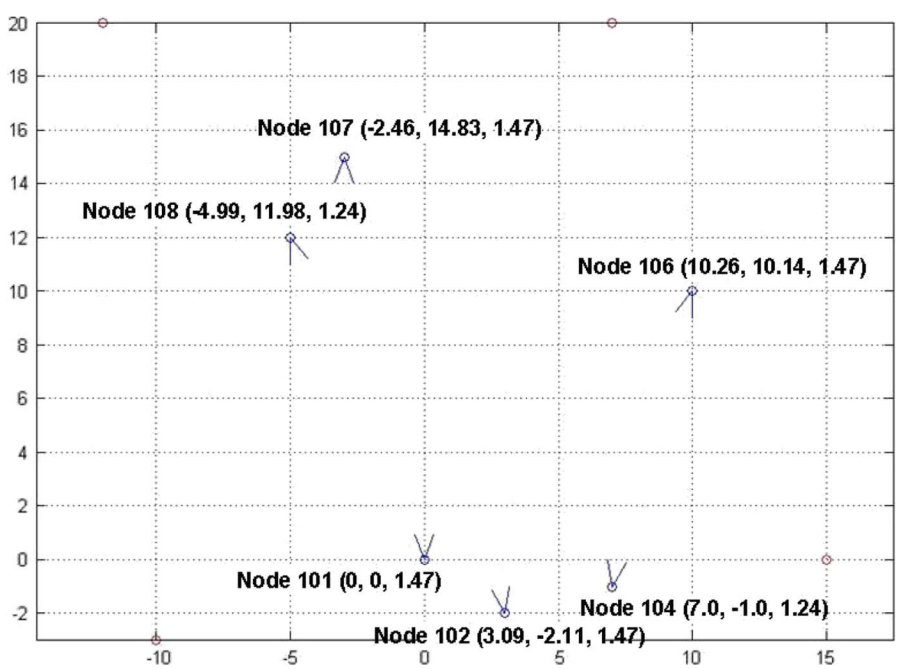

Fig. 12. ***An overhead view of the layout of the cameras+radio sensors. The units are measured in meters.***

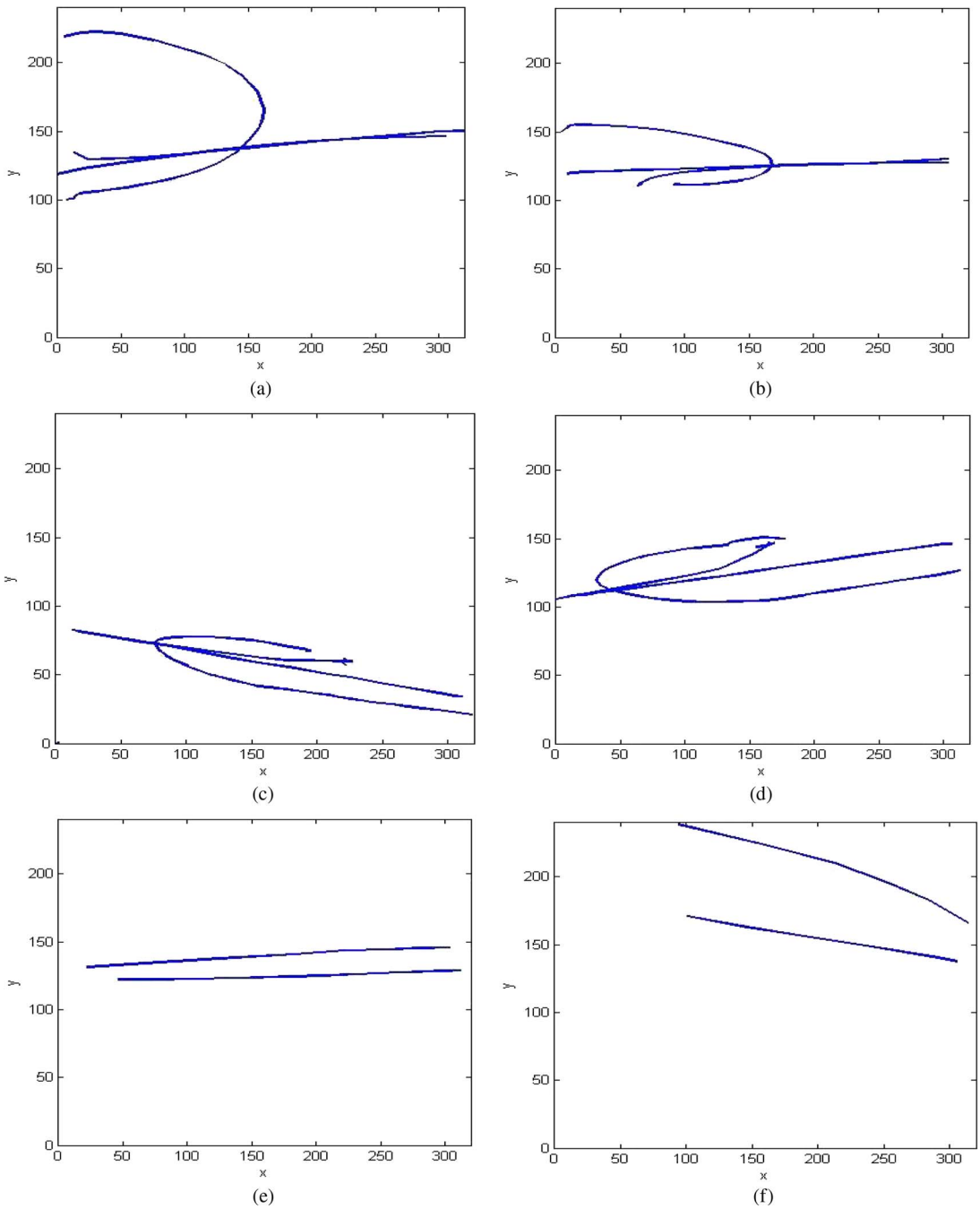

Fig. 13. ***(Cameras 101, 102, 107, and 108) Detected tracks for frames 1 through 500 for cameras which had correspondence in their respective tracks. (Cameras 104 and 106) Detected tracks for frames 1 through 500 for cameras that did not have correspondence with the top row cameras, but which had correspondence with each other. (a) Camera 101. (b) Camera 102. (c) Camera 107. (d) Camera 108. (e) Camera 104. (f) Camera 106.***

given the correspondence between object image tracks. It shows that cameras 104 and 106 are disjoint from the rest of the network. While their fields of view overlap with each other, they are not connected to the rest of the network. We verified that that was correct based on the ground truth of the setup. The average reprojection error for all camera pairs is less than 1 pixel.

Using the radio interferometry method, we compute translations for all overlapping camera pairs. Then, we developed both nonlinear and linear methods for solving a complete localization of a camera network, finding both the orientation of the fields of view of each camera as well as the positions of cameras including scale factors (see [54] for more detail). The resulting scale factors are shown in

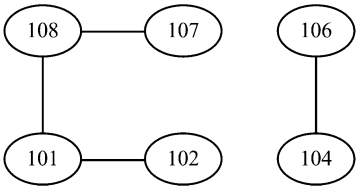

Fig. 14. ***The overlap in fields of view between the camera nodes based on the object image tracks.***

Table 3. It should be noted that the linear method solves for all scaling factors even if the camera pair does not have overlapping fields of view.

IV. UAV SWARMS AND MULTIAGENT COORDINATION

UAVs have been proven as effective and affordable solutions that complement many operations traditionally performed by humans. Currently, UAVs are only deployed in solo missions, managed by a number of well-trained operators. However, owing to fast technical advances in navigation, control, and communication, a group of autonomous mobile agents are expected to execute complex missions in dynamic situations in the near future. In such scenarios, a group of autonomous agents will be able to carry out complex missions as a collective entity so that, even if some members of the team become ineffective, the surviving members of the team can still accomplish the given mission by reallocating tasks to the surviving members. When deploying a group of UAVs into the field of action, they should fly without any collision with other agents or obstacles, stationary or moving, along their paths. Planning a collision-free path for single agent in a perfectly known environment is a well-investigated problem and there are many efficient algorithms available [58]. However, solving for collision-free paths for multiple UAVs in dynamic environment demands replanning capability literally *on the fly* by actively taking the latest sensing information into account. In the following, for the scenarios of deploying a swarm of UAVs in a realistic environment, we propose a hierarchical structure to guide a group of vehicles without any collision by combining the information collected by onboard sensors with geographic information database available prior to the mission.

TABLE 3 The Scale Factors for the Distances Between Cameras

Camera Pair	Ground Truth	Nonlinear Estimate	Linear Estimate
101 to 102	3.7417	3.2376	4.2593
101 to 107	15.0326	15.5074	13.5940
101 to 108	12.9797	13.2370	13.1016
102 to 107	17.8260	15.4361	14.9415
102 to 108	16.2440	–	15.4440
107 to 108	3.8179	3.6743	1.5795

A. System Architecture

For swarming scenarios in a complex environment, we propose a hierarchical system that consists of a global path planner as the upper layer and a local trajectory replanner as the lower layer. In this approach, based on the mapping information collected prior to a mission, the path planner initially generates reference trajectories for each vehicle that lead to the destination without any conflict with known obstacles. When the agents are deployed, the local planner on each agent repeatedly solves for a conflict-free trajectory based on the latest information on the locations of nearby vehicles and any unexpected obstacles, which is collected using onboard sensors and intervehicular communication. For trajectory replanning, we propose a model-predictive approach [35], [36], which solves for a trajectory that minimizes the cost function that penalizes the tracking error and the collision with other vehicles and obstacles over a finite time in the future. The trajectory replanner resides on each vehicle and computes for a collision-free trajectories using the obstacle information collected by onboard sensors of its own or from other vehicles if possible. The proposed system architecture is illustrated in Fig. 15.

B. MPC Formulation

In this section, we formulate an MPC-based trajectory planner. Suppose we are given a nonlinear time-invariant dynamic system such that

$$\begin{aligned} x(k+1) &= f(x(k)) + g(x(k))u(k) \\ y(k) &= h(x(k)) \end{aligned} \tag{1}$$

where $x \in X \subset \mathbb{R}^{n_x}$, $u \in U \subset \mathbb{R}^{n_u}$. The optimal control input sequence over the finite receding horizon N is obtained by solving the following nonlinear programming problem:

$$\begin{aligned} \text{Find} \quad & u(k), \qquad k = i, i+1, \ldots, i+N-1 \\ \text{such that} \quad & u(k) = \arg\min V(x,k,u) \end{aligned} \tag{2}$$

where

$$V(x,k,u) = \sum_{i=k}^{k+N-1} L(x(i),u(i)) + F(x(k+N)). \tag{3}$$

Here, L is a positive-definite cost function and F is the terminal cost. Suppose $u^*(k)$, $k = i, \ldots, i+N-1$, is the

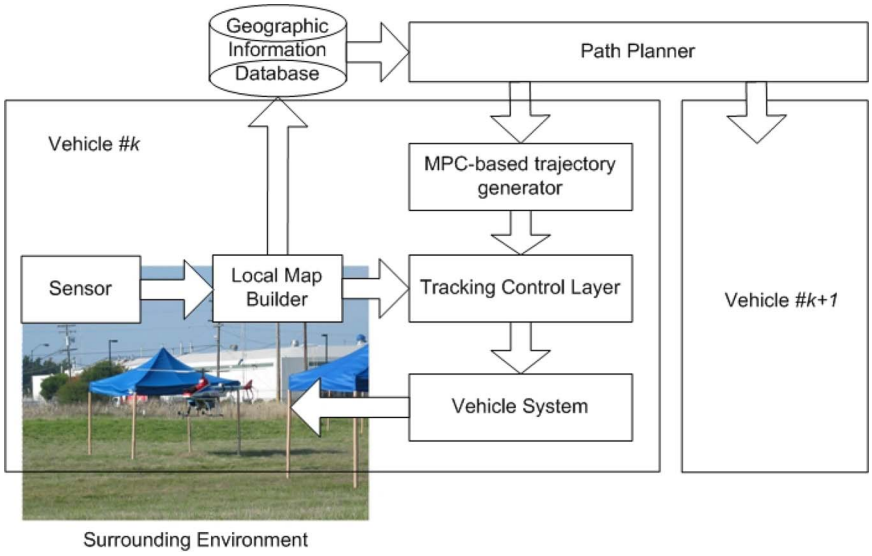

Fig. 15. ***System architecture of a swarming algorithm scenario.***

optimal control sequence that minimizes $V(x,k,u)$ such that $V^*(x,k) \triangleq V(x,k,u^*(x,k)) \leq V(x,k,u), \quad \forall u(k) \in U$. The cost function term L is chosen such that

$$L(x,u) = \frac{1}{2}(x^r - x)^T Q(x^r - x) + \frac{1}{2}u^T R u + S(x) + \sum_{l=1}^{n_o} P(x,\eta_l). \quad (4)$$

The first term in (4) penalizes the deviation from the original trajectory denoted as x^r. The second term penalizes the control input. $S(x)$ is the term that penalizes any states not in X as suggested in [36]. $P(x_v,\eta_l)$ is the term to implement the collision avoidance capability in this MPC framework. As will be explained in further detail below, $P(x_v,\eta_l)$ increases with bound as $\|x_v - \eta_l\|_2 \to 0$, where $x_v \in \mathbb{R}^3$ is the position of the vehicle and η_l is the coordinates of the lth obstacle from a total of n_o obstacles. During online optimization, the control input can be enforced to explicitly meet the saturation requirement by enforcing

$$u_i(k) = \begin{cases} u_i^{\max}, & \text{if} \quad u_i > u_i^{\max} \\ u_i^{\min}, & \text{if} \quad u_i < u_i^{\min} \end{cases} \quad (5)$$

where $u \triangleq [u_1 \ \ldots \ u_{n_u}]^T$. In this manner, one can find the control input sequence that will be always within the physical limit of the given dynamic system. We use the optimization method based on the indirect method of Lagrangian multipliers suggested in [59].

C. Obstacle Sensing and Trajectory Replanning

For a swarming scenario, it is very important to know where the nearby vehicles are located. Due to the large number of agents, it is highly desired to sense those using onboard sensors, not receiving the broadcast information on a wireless communication channel. Obstacle detection can be done in either active or passive manner and the choice depends on many factors including operating condition, accuracy, and maximum detection range. Laser scanners measure the distance to an object by precisely measuring the time of flight of a laser beam to return from a target. It can be very accurate and straightforward, so it is favored for 3-D mapping. The detection range depends on the intensity of the light that radiates from the laser source. Active radar has similar attributes since it operates in a similar principle: however, its resolution is much lower while the detection range can be significantly longer. Both methods may not be suitable if the mission should be a covert one. For such cases, vision-based methods are favored as it is a passive sensing method and can offer a far greater amount of information if processed adequately.

For collision avoidance, we choose $P(x_v,\eta_l)$ in (4) such that

$$P(x_v,\eta_l) = \frac{1}{(x_v - \eta_l)^T G (x_v - \eta_l) + \varepsilon} \quad (6)$$

where G is positive definite and $\varepsilon > 0$ is to prevent ill conditioning when $\|x_v - \eta_l\|_2 \to 0$. One can choose $G = \mathrm{diag}\{g_x, g_y, g_z\}$, $g_i > 0$, for an orthogonal penalty function. The penalty function (6) serves as a repelling

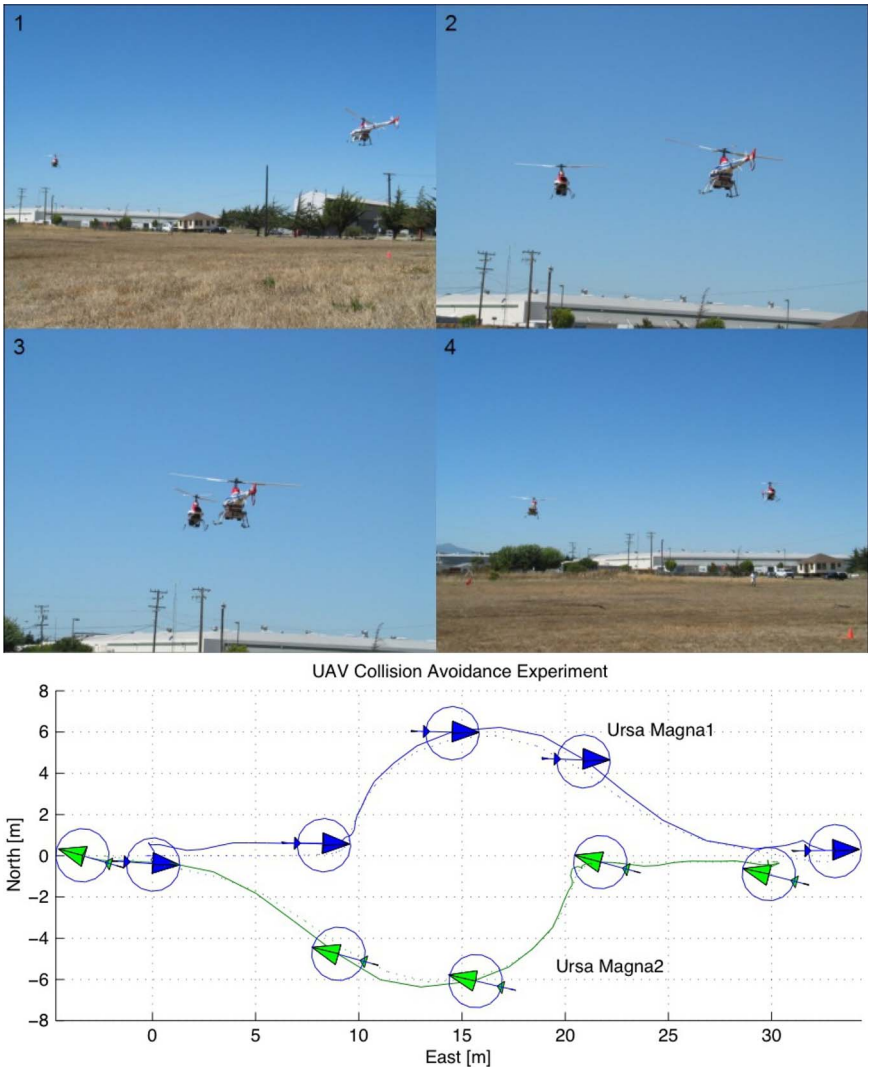

Fig. 16. ***Midair collision avoidance between two rotorcraft UAVs using real-time MPC and the trajectories of two helicopters.***

potential field and has nonzero value for entire state space even when the vehicle is far enough from obstacles. The key advantage over conventional potential field approach here is that we optimize over a finite receding horizon, not only for the current time as in the potential field approach. For obstacle avoidance, we consider two types of scenarios: 1) a situation when the vehicle needs to stay as far as possible from the obstacles even if no direct collision is anticipated and 2) a situation when the vehicle can be arbitrarily close to the obstacle as long as no direct conflict is caused. For the second situation, one can choose to enable (6) only when $\|x_v - \eta_l\|_2 < \sigma_{\min}$, where $\sigma_{\min}$ is the minimum safety distance from other vehicles.

Since MPC algorithms optimize over a receding finite horizon into the future, for moving obstacles, their predicted trajectories over $k = i, i+1, \ldots, i+N-1$, are needed in (6). It is observed that the inclusion of predicted obstacle locations in the optimization will produce more efficient evasion trajectory provided that the prediction is reasonably accurate. The simplest yet reasonable estimation is the extrapolation using the current position and velocity over the prediction horizon such that

$$\eta_l(k+i) = \eta_l(k) + \Delta t v_l(k)(i-1). \tag{7}$$

It is noted that the prediction can be done in more elaborated manners using a Kalman filter, exploiting any knowledge on the motion of obstacles if available.

D. Experiment Results

1) Intervehicular Collision Avoidance: As the first logical step, we consider an exemplary scenario of two UAVs

exercising identical evasion strategies to demonstrate the viability of the proposed algorithm in real situations. The proposed algorithm was implemented on MATLAB Simulink and tested on a team of two helicopter UAVs. The detailed specifications and architecture are explained in [35]. In this experiment, Simulink was configured to run in real time and sent the trajectory commands over a radio link so that the UAVs followed the designated path by the onboard flight controller. The vehicles broadcast their location using GPS to the ground station, where the MPC-based trajectories were generated in a centralized manner. The experiment result is shown in Fig. 16. Two vehicles are configured to fly towards each other following a head-on collision course. In this particular case, the vehicles are constrained to make evasive moves only in the horizontal plane as a safety measure although the proposed algorithm is fully capable of vertical evasion as well. Both vehicles are also executing the same evasive algorithm. As can be seen from Fig. 16, the vehicles are able to pass by each other with a sufficient safety clearance.

2) Obstacle Avoidance: As a next step, we consider an autonomous exploration problem in an urban environment, which was simulated by a field with portable canopies ($3 \times 3 \times 3$ m^3). They were arranged as shown in the picture in Fig. 17. The distance between the neighboring canopies was set to 10–12 m so that the test UAV with 3.5-m-long fuselage could pass between the canopies with minimal safe clearance, about 3 m from the rotor tip to the nearby canopy when staying on course. For validation, the MPC engine developed in [36] was applied to the proposed urban experiment setup. A simulation model was constructed in MATLAB/Simulink, where the local map building with a laser scanner was substituted with a preprogrammed map. The MPC algorithm with the local map building algorithm was implemented in C language for computation speed and portability. For this experiment, the Simulink model used in the collision avoidance was modified and ran for real-time trajectory generation at 10 Hz.

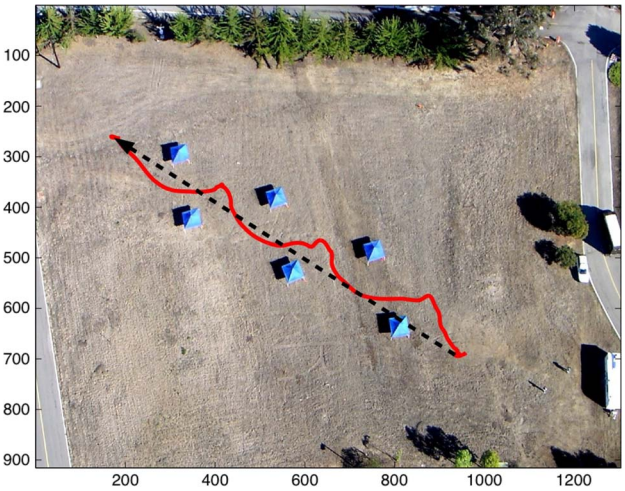

Fig. 17. ***Aerial view of urban navigation experiment (dashed: given straight path, solid: actual flight path of UAV during experiment).***

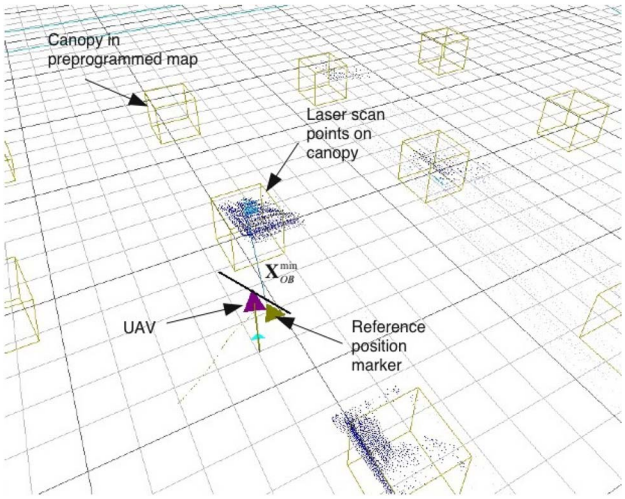

Fig. 18. ***A snapshot of 3-D rendering during an urban exploration experiment.***

As shown in Fig. 17, the MPC path planner is capable of generating a collision-free trajectory around the buildings based on the original trajectory, which intentionally intersects with some buildings.

Urban exploration experiments were performed using the same Berkeley UAV testbed used in the intervehicular collision avoidance experiment. This time, for obstacle detection, the vehicle was equipped with an LMS-200 from Sick AG, a 2-D laser range finder. It offers maximum 80-m scanning range with 10-mm resolution and weighs 4.5 kg. The measurement was sent to the flight computer via RS-232 and then relayed to the ground station running the MPC-based trajectory generator in Simulink. The laser scanner data were then processed following the method proposed in Section IV-B. In Fig. 18, a 3-D rendering from the ground station software is presented. The display shows the location of the UAV, the reference point marker, to a point in the local obstacle map at that moment, and laser-scanned points as blue dots. During the experiments, the laser scanner used in our experiment demonstrated its capability to detect the canopies in the line of sight with great accuracy, as well as other surrounding natural and artificial objects including buildings, trees, and power lines.

The processed laser scanned data in a form of local obstacle map were used in the optimization (2) to generate a trajectory using the algorithm in Section IV-C. The trajectory was then sent via IEEE 802.11b to the avionics system with a dedicated process running to enforce the

command update rate at 10 Hz. The tracking control layer enabled the host vehicle to follow the given trajectory with sufficient distance. In a series of experiments, the vehicle was able to fly around the obstacles with sufficient accuracy for tracking the given trajectory, as shown in Fig. 17 (red line).

E. Cooperative Multiagent Coordination

The pursuit-evasion game is a probabilistic game scenario, whose goal is to "catch," in a finite time, evaders in a given field with pursuers, which are commanded by some pursuit algorithms. The initial locations of evaders are unknown. The pursuers build probabilistic maps [31] of the possible locations of evaders using their sensing devices, which are typically vision based. In this scenario, the group of pursuers, consisting of UAVs and/or UGVs, is required to go to the requested waypoints, take measurements of the location of themselves and of any evaders within its detection range, and report the measurement as well as their current locations. This measurement is used

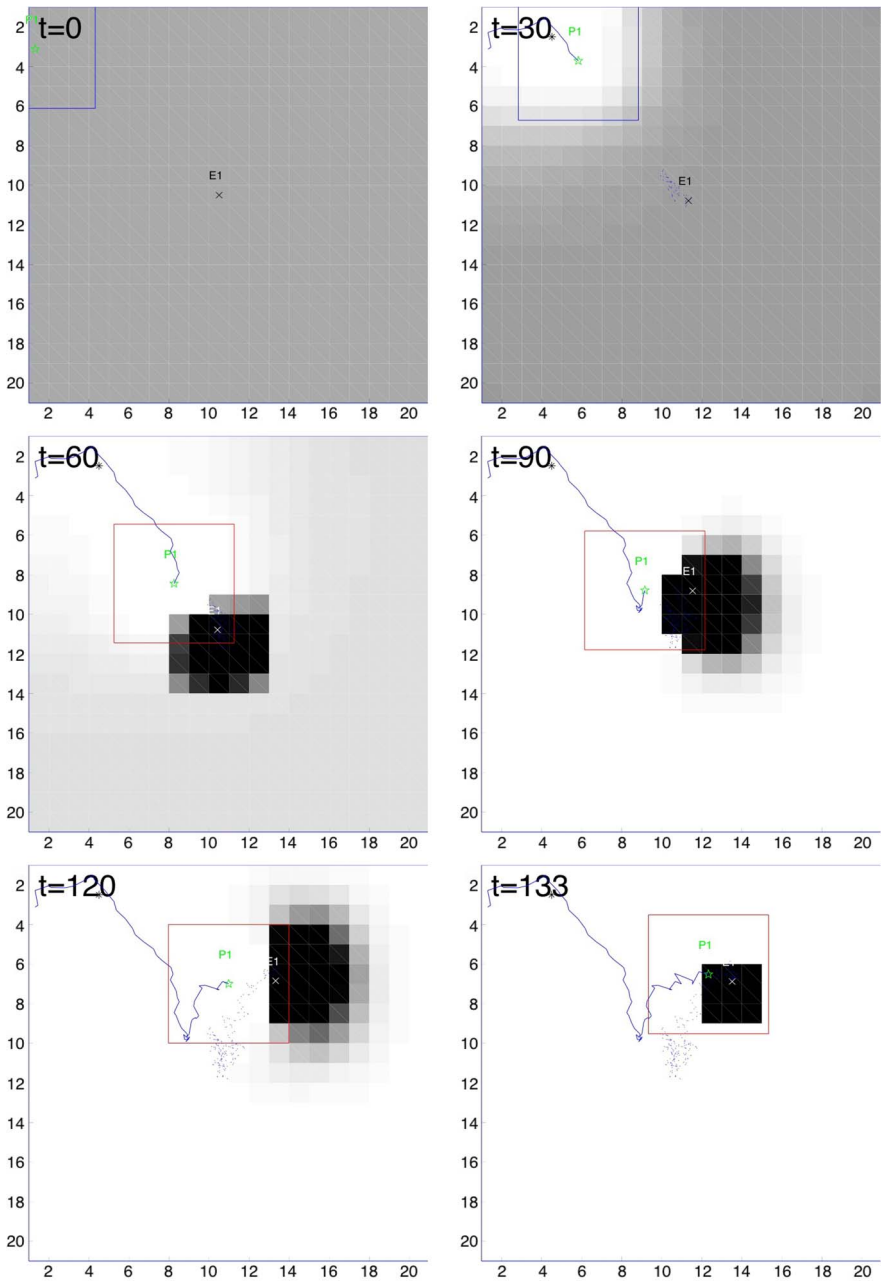

Fig. 19. ***A PEG between one pursuer and one evader (×: evader; ∗: pursuer; background: probabilistic map; darker region represents a higher probability for capturing the evader).***

to compute the waypoint of pursuers at next time frame and sent to the pursuers via wireless communication for tracking. In the experiment setup, the PEG algorithm was implemented in MATLAB/Simulink in a similar manner with the previous experiments.

In Fig. 19, a result from a PEG game with one aerial pursuer versus one ground evader is shown. It is noted that the number of participating pursuers and evaders can be easily changed although only one pursuer and one evader exist in this example to maximize the role of the aerial pursuer UAV. When the game starts, the UAV maintains hover, waiting for the starting signal from the PEG server. The ground robot roams in the given field of 20 m $\times$ 20 m. The graph shows two trajectories: one for the pursuer UAV and the other for the evader UGV. The snapshots in Fig. 19 show the progress of PEG in time. Along with the trajectories, it also shows the probabilistic map shown as the gray-scale background and the visibility region denoted as a square. The evader is caught in 133 s after the game is started.

F. Towards a Swarm of UAVs in Cluttered Environment

In order to evaluate the proposed hierarchical system for swarming of UAVs, we consider a scenario where 16 UAVs are to be deployed into an urban environment. Fig. 20 shows an aerial photograph of Fort Benning, GA, where the scenario takes place. The geometry of buildings and their locations are known *a priori*. In this area, some of corridors that the UAVs are required to fly through are as narrow as 5 m. Therefore, the scenario calls for small-size rotorcraft UAVs that can fit into the area and fly slowly and accurately enough. In this scenario, 16 helicopter UAVs are initially flying in a four by four formation, toward the designated cells. Then, they divide into three subgroups. Some of these subgroups ingress into the area below the roof line (teams A and C) between the buildings while others fly over the roof top (team B).

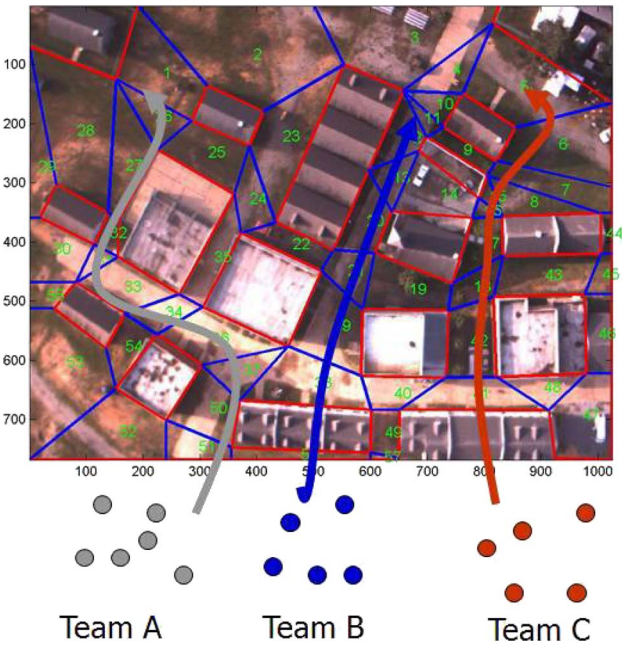

Fig. 20. ***An aerial photograph of Fort Benning, GA. UAVs in three teams are commanded to fly to the designated cells marked with a serial number.***

For this scenario, the path planner computes initial paths that are clear from the buildings, but not necessarily from other agents. In fact, if we were to consider the intervehicular conflict at the initial planning, the computation can be not only heavy due to numerical iterations computing an optimal solution but also not useful at all if any vehicle deviates from the initial planning due to any unforeseen events occurring. The model-predictive layer plays an important role here when such events occur; the online trajectory layer solves for a safe trajectory by minimizing the cost function that penalizes the near-collision conditions.

The simulation was also implemented using MATLAB and Simulink. Sixteen Simulink blocks of a detailed helicopter model with 15 state variables and nonlinear kinematics matched with a MPC solver were built and ran in parallel during the simulation. The vehicles' positions were shared among the 16 blocks, assuming the existence of a communication channel that broadcast the position information at the sampling rate of 25 Hz, which was deemed rather fast in reality. We imposed a 30-m sensing limit of other agents. Since the model-predictive algorithm was numerically heavy, it was implemented using the CMEX feature of Simulink to speed up. The core algorithm was constructed to be compatible with CMEX and the flight control software in C/C++ so that the code validated in MATLAB could be readily ported into the actual flight software. Test results show that the implemented model-predictive algorithm is capable of running in real time on a Pentium III 700-MHz core of an industrial PC board known as PC-104 [60].

The simulation result is given in Fig. 21. Initially, the helicopter UAVs fly at 10 m/s in a loose four by four formation [Fig. 21(a)] where the trajectory generator only considers the tracking of the reference path segment generated by the path planner offline and the collision avoidance with other agents. Then, just before they enter the town, they are divided into three subgroups. This behavior is achieved by generating a common reference path for each team. The collision-aware tracking capability commands each vehicle to divide into three subgroups without any collision [Fig. 21(c)]. As they approach the area with fixed obstacles, i.e., the buildings, the collision avoidance term (7) in (2) begins to increase. In this simulation, since the algorithm is fully decentralized, the vehicles sometimes show "shopping mob"-like behavior: as one vehicle is about to enter the corridor, due to the

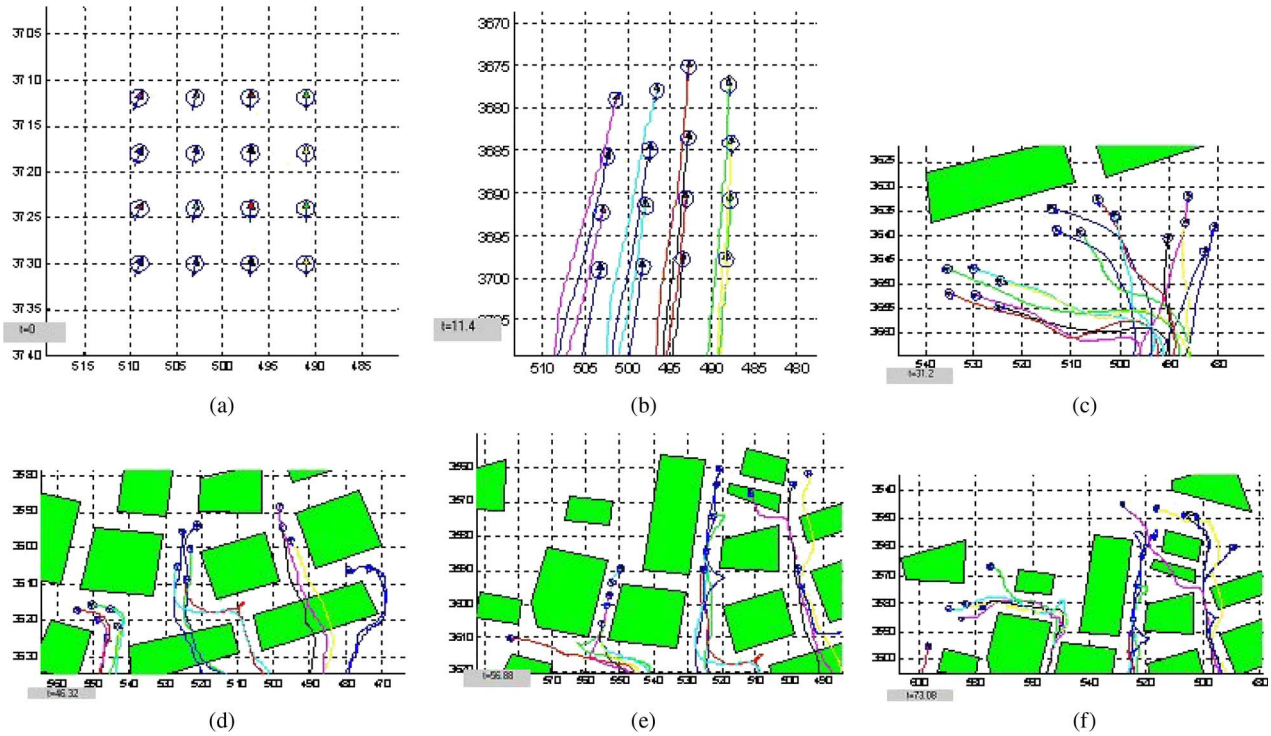

Fig. 21. ***Simulation result of a swarming into an urban area shown in Fig. 20. (a) $t = 0$; (b) $t = 11.4$; (c) $t = 31.2$; (d) $t = 45.3$; (e) $t = 56.9$; (f) $t = 73.1$.***

collision avoidance cost, it is pushed away by following vehicles from the opening of the corridor while the followers succeed to enter the corridor. This observation suggests a coordination among neighboring UAVs may be necessary for more efficient deployment. In Fig. 21(f), all UAVs arrive at their destinations without any collision.

G. External Active-Set Methods for Constrained MPC-Based Guidance

Modeling obstacles as potential functions described in the previous sections is more convenient to implement, and it enables a decentralized computation scheme. However, it suffers from a scaling issue when there are too many obstacles, therefore too many potential functions, to be considered in the objective function (4). Also, in applications where safety is critical, regarding the collision avoidance as explicit state-space constraints is preferable.

The optimal control problems with state-space constraints for MPC-based guidance of vehicles are characterized by large numbers of collision avoidance inequalities and by expensive evaluations of the gradients of these inequality-defining functions. Since potential collisions are confined to relatively short segments of the UAV trajectories, most of the collision avoidance inequalities are inactive. In the case of UAVs, the sampling intervals are short and hence the viability of the MPC scheme is largely determined by the speed of the nonlinear programming solvers.

Unfortunately, most standard nonlinear programming packages, including the excellent set found in TOMLAB [61], including SNOPT [62], NPSOL [63], and Schittkowski SQP [64], are not designed to exploit the fact that a problem with a large number of nonlinear inequality constraints may have few active constraints.

Based on these observations, we have developed an accelerator scheme for general nonlinear programming packages, based on the theory of outer approximations (see [65, p. 460]), which acts as an *external* active constraint set strategy for solving nonlinear programming problems with a large number of inequality constraints. This strategy constructs a finite sequence of inequality constrained nonlinear programming problems, containing a progressively larger subset of the constraints in the original problem, and submits them to a nonlinear programming solver for a fixed number of iterations. We have proved that this scheme computes a solution of the original problem and showed, by means of numerical experiments, that when applied to a finite-horizon optimal control problem (FHOCP) with a large number of state-space constraints, this strategy results in reductions in computing time ranging from a factor of 6 to a factor of over 100.

In the following, we apply our external active-set method to the MPC-based guidance of multiple UAVs with collision avoidance and no-flight zone constrains, and show the effectiveness of our scheme.

1) External Active-Set Algorithm: Consider the inequality constrained minimization problem

$$\mathbf{P_q}: \quad \min\{f^0(\eta)|f^j(\eta) \le 0, j \in \mathbf{q}\} \tag{8}$$

where $\eta \in \mathbb{R}^n$, and $\mathbf{q} \triangleq \{1, \ldots, q\}$. We assume that functions $f^j : \mathbb{R}^n \to \mathbb{R}$ are at least once continuously differentiable. In the context of discrete optimal control problems, η can be either a discretized control sequence or an initial state–discretized control sequence pair.[2]

Next we define the index set $\mathbf{q}_\epsilon(\eta)$ with $\epsilon > 0$ by

$$\mathbf{q}_\epsilon(\eta) \triangleq \{j \in \mathbf{q}|f^j(\eta) \ge \psi_+(\eta) - \epsilon\} \tag{9}$$

where

$$\psi(\eta) \triangleq \max_{j\in\mathbf{q}} f^j(\eta) \tag{10}$$

and

$$\psi_+(\eta) \triangleq \max\{0, \psi(\eta)\}. \tag{11}$$

Definition IV.1: We say that an algorithm defined by a recursion of the form

$$\eta_{k+1} = A(\eta_k) \tag{12}$$

for solving inequality constrained problems of the form (8) is *convergent* if any accumulation point of a sequence $\{\eta_i\}_{i=0}^{\infty}$, constructed according to the recursion (12), is a feasible stationary point.

Finally, we assume that we have a convergent algorithm for solving inequality constrained problems of the form (8), represented by the recursion function $A(\cdot)$, i.e., given a point η_k the algorithm constructs its successor η_{k+1} according to the rule (12).

[2]See [66, Ch. 4] for a detailed treatment of discrete time optimal control problems.

Algorithm IV.1
Active-Set algorithm for inequality constrained minimization problems.

Data: η_0, $\epsilon > 0$, $N_{\text{iter}} \in \mathbb{N}$
Step 0: Set $i = 0$, $\mathbf{Q}_0 = \mathbf{q}_\epsilon(\eta_0)$.
Step 1: Set $\zeta_0 = \eta_i$ and perform N_{iter} iterations of the form $\zeta_{k+1} = A(\zeta_k)$ on the problem

$$\mathbf{P}_{\mathbf{Q}_i} \quad \min\{f^0(\zeta)|f^j(\zeta) \le 0, j \in \mathbf{Q}_i\} \tag{13}$$

to obtain $\zeta_{N_{\text{iter}}}$ and set $\eta_{i+1} = \zeta_{N_{\text{iter}}}$.
Step 2: Compute $\psi(\eta_{i+1})$.
if $\zeta_{N_{\text{iter}}}$ is returned as a global, local, or stationary solution of $\mathbf{P}_{\mathbf{Q}_i}$ and $\psi(\eta_{i+1}) \le 0$, **then**
STOP
else
Compute

$$\mathbf{Q}_{i+1} = \mathbf{Q}_i \cup \mathbf{q}_\epsilon(\eta_{i+1}) \tag{14}$$

and set $i = i + 1$, and go to Step 1.
end if

In [38], we have shown that the stationary point computed by Algorithm IV.1 is also a stationary point of the original problem, which is summarized in the following theorem.

Theorem IV.1: Suppose that the problem $\mathbf{P_q}$ has feasible solutions, i.e., there exist vectors η^* such that $f^j(\eta^*) \le 0$ for all $j \in \mathbf{q}$.

a) If Algorithm IV.1 constructs a finite sequence $\{\eta_i\}_{i=0}^{k}$, exiting in Step 2, with $i + 1 = k$, then η_k is a global, local, or stationary solution for $\mathbf{P_q}$, depending on the exit message from the solver defined by $A(\cdot)$.
b) If $\{\eta_i\}_{i=0}^{\infty}$ is an infinite sequence constructed by Algorithm IV.1 in solving $\mathbf{P_q}$, then any accumulation point[3] $\hat{\eta}$ of this sequence is feasible and stationary for $\mathbf{P_q}$.

Although the above theorem guarantees that our algorithm converges to a stationary solution of the original problem, it does not tell much about its performance when it is used in an MPC scheme. In [38], we showed that our algorithm reduced the computation time dramatically in solving a state-constrained FHOCP.

[3]A point $\hat{\eta}$ is said to be an accumulation point of the sequence $\{\eta_i\}_{i=0}^{\infty}$ if there exists an infinite subsequence, indexed by $K \subset \mathbb{N}$, $\{\eta_i\}_{i\in K}$, such that $\eta_i \xrightarrow{K} \hat{\eta}$ as $i \xrightarrow{K} \infty$

2) Numerical Example: In this section, we apply the external active-set algorithm to an MPC-based guidance problem, and compare the computation time with that of "native" case, in which a nonlinear solver without our algorithm was used. We consider the problem of controlling four identical UAVs which are required to fly, along a circular trajectory in a horizontal plane, without incurring a collision, for an indefinite period of time. The circular trajectory is obstructed by no-flight zones that are described by ellipses. Their controls over a control time horizon T_s are to be determined by a centralized computer, by solving an FHOCP with the prediction horizon length T.

For the sake of simplicity, we assume that each UAV flies at a constant speed v and that the scalar control u_i, for the ith UAV determines its rate of heading angle change in radians per second. The cost function for this problem is proportional to the sum of the energy used by the UAVs over the interval $[0, T]$ and the sum of distance to the circular trajectory at the end of the prediction horizon, i.e.,

$$f^0(u) \triangleq \sum_{i=1}^{4} \left\{ \int_0^T \frac{1}{2} u_i^2(\tau)\, d\tau + wC(x_i(T)) \right\} \tag{15}$$

where $C(x_i(T)) \triangleq x_i^1(T)^2 + x_i^2(T)^2 - r_d^2$, the square of the distance error between the final vehicle position at $t = T$ and the desired circular trajectory, w is the weighting factor, $u \triangleq (u_1, u_2, \ldots, u_4)$, and r_t is the radius of the desired circular trajectory. (x_i^1, x_i^2) denotes the position coordinates of the ith UAV on a plane, and x_i^3 denotes the heading angle in radian of the ith UAV, respectively. The constraints are those of staying outside the no-flight zones and avoiding collisions with other vehicles.

In order to state the optimal control problem as an endpoint problem defined on [0, 1], we rescale the state dynamics of each UAV using the actual terminal time T and augment the 3-D physical state (x_i^1, x_i^2, x_i^3) with a fourth component x_i^4

$$x_i^4(t) \triangleq \int_0^t \frac{T}{2} u_i^2(\tau)\, d\tau \tag{16}$$

which represents the energy used by the ith UAV. The resulting dynamics of the ith UAV have the form

$$\frac{dx_i(t)}{dt} = \begin{bmatrix} Tv\cos x_i^3(t) \\ Tv\sin x_i^3(t) \\ Tu_i(t) \\ \frac{T}{2} u_i(t)^2 \end{bmatrix} \triangleq h(x_i(t), u_i(t)) \tag{17}$$

with the initial state $x_i(0)$ given. In spite of its simplicity, this model describes quite well the dynamics of a fixed-wing aircraft, whose attitude, altitude, and forward speed are stabilized by an autopilot. It was used in other papers, including air traffic management [66], and UAV trajectory planning [67]. We will denote the solution of the dynamic (17) by $x_i(t, u_i)$, with $t \in [0, 1]$.

Based on the scaled state dynamics, the optimal control problem we need to solve is of the form

$$\min_{u \in L_\infty^4[0,1]} f^0(u) \tag{18}$$

where

$$f^0(u) \triangleq \sum_{i=1}^{4} \left\{ x_i^4(1, u_i) + wC(x_i(1, u_i)) \right\} \tag{19}$$

subject to two sets of constraints

a) no-flight zone constraints

$$f_{\mathrm{nf}}^i(t, u_i) \triangleq G_j\big(x_i(t, u_i), x_c, a_j, b_j, \phi_j\big) \le 0 \tag{20}$$

$\forall t \in [0, 1]$, $i = 1, \ldots, 4$, $j = 1, \ldots 4$;

b) pairwise collision avoidance constraints

$$\begin{aligned} f_{\mathrm{ca}}^{(i,j)}(t, u_i, u_j) \triangleq & \left(x_i^1(t, u_i) - x_j^1(t, u_j)\right)^2 \\ & + \left(x_i^2(t, u_i) - x_j^2(t, u_j)\right)^2 \\ \ge & \, r_{\mathrm{ca}}^2 \end{aligned} \tag{21}$$

$\forall t \in [0, 1]$, $i \ne j$, $i, j = 1, \ldots, 4$. $G_j(x_i(u_i), x_{cj}, a_j, b_j, \phi_j)$ is the constraint function for the jth no-flight zone that is described by an ellipse centered at x_{cj}, rotated counterclockwise by ϕ_j, with the values of major and minor axes a_j and b_j, respectively.

To solve this problem, we must discretize the dynamics. We use Euler's method to obtain

$$\bar{x}_i(t_{k+1}) - \bar{x}_i(t_k) = \Delta h(\bar{x}_i(t_k), \bar{u}_i(t_k)) \tag{22}$$

with $\bar{x}_i(0) = x_i(0)$, $i = 0, 1, \ldots, 4$, $\Delta \triangleq 1/N$, $N \in \mathbb{N}$, $t_k \triangleq k\Delta$, and $k \in \{0, 1, \ldots, N\}$. We use an overbar to distinguish between the exact variables and the discretized variables. We will denote the solution of the discretized dynamics by $\bar{x}_i(t_k, \bar{u}_i)$, $k = 0, 1, \ldots, N$, with

$$\bar{u}_i \triangleq (\bar{u}_i(t_0), \bar{u}(t_1), \ldots, \bar{u}_i(t_{N-1})). \tag{23}$$

Finally, we obtain the following discrete-time optimal control problem:

$$\min_{\bar{u}_i \in \mathbb{R}^N, i \in \{1,\ldots,4\}} \bar{f}^0(\bar{u}) \tag{24}$$

where

$$\bar{f}^0(\bar{u}) \triangleq \sum_{i=1}^{4} \left\{ \bar{x}_i^4(1,\bar{u}_i) + \bar{x}_i^1(1,\bar{u}_i)^2 + wC(x_i(1,\bar{u}_i)) \right\} \tag{25}$$

subject to $|\bar{u}_i(t_k)| \leq c$, the discretized dynamics of each UAV (22), and the discretized no-flight zone and collision avoidance constraints

$$\bar{f}_{\mathrm{nf}}^{i,k}(\bar{u}_i) \triangleq G_j\big(\bar{x}_i(t_k,\bar{u}_i), x_c, a_j, b_j, \phi_j\big) \leq 0 \tag{26}$$

for $k = 0, 1, \ldots, N-1$ and $i = 1, 2, \ldots, 4$, and

$$\begin{aligned} f_{\mathrm{ca},(i,j)}^k(\bar{u}_i,\bar{u}_j) &\triangleq \left(\bar{x}_i^1(t_k,\bar{u}_i) - \bar{x}_j^1(t_k,\bar{u}_j)\right)^2 \\ &\quad + \left(\bar{x}_i^2(t_k,\bar{u}_i) - \bar{x}_j^2(t_k,\bar{u}_j)\right)^2 \\ &\geq r_{\mathrm{ca}}^2 \end{aligned} \tag{27}$$

$\forall k \in \{1,\ldots,N\}$, $i \neq j$, $i,j = 1,\ldots,4$. The total number of nonlinear inequality constraints in this problem is $4N(4-1)/2 + 4 \cdot 4N = 22N$.

The numerical experiments were performed using MATLAB V7.6 and SNOPT 6.2 [62] in TOMLAB V7.1 [61]. We used a desktop with two AMD Opertron 2.2-GHz processors with 8-GB RAM, running Linux 2.6.28. Although we used a computer with multicore central processing units (CPUs), it was observed that only one core was used by our computation. In the numerical experiments, the reference trajectory was generated by the following algorithm.

Algorithm IV.2
MPC-based guidance algorithm

Set $k = 0$.
Data: x_0, and the initial reference trajectory $x^{\mathrm{ref}}_{[t_{k+1},t_{k+N_c-1}]} \triangleq (\bar{x}(t_{k+1}),\ldots,\bar{x}(t_{k+N_c}))$.
Step 1: Output $x^{\mathrm{ref}}_{[t_k,t_{k+N_c}]}$ to the low-level tracking controller
Step 2: Set $x(0) = x^{\mathrm{ref}}(t_{k+N_c})$ and solve the discrete-time FHOCP (24) to obtain $\bar{u}_{[t_k,t_{k+N_c-1}]} \triangleq (\bar{u}(t_k),\bar{u}(t_{k+1}),\ldots,\bar{u}(t_{k+N_c-1}))$.
Step 3: Compute the reference state trajectory $x^{\mathrm{ref}}_{[t_{k+1},t_{k+N_c-1}]}$ using $\bar{u}_{[t_k,t_{k+N_c-1}]}$.
Step 4: Wait until $t = t_{k+N_c}$.
Step 5: Set $k = k+1$ and go to Step 1.

The algorithm implicitly requires that the solution be computed within $N_c\Delta$.

We set $v = 16$ m/s, $r_{\mathrm{d}} = 320$ m, $r_{\mathrm{ca}} = 16$ m, $c = 0.5$ rad/s, $w = 0.01$, and $N_{\mathrm{iter}} = 10$. We fixed $\Delta = 5/16$ and $N_c = 18$, which means a solution of the FHOCP (24) should be computed within $\Delta N_c = 5.625$ s. Initial conditions are

$$\begin{aligned} x_1(0) &= \left(-376, 280, -\frac{\pi}{4}, 0\right) \\ x_2(0) &= \left(56, 448, -\frac{3\pi}{4}, 0\right) \\ x_3(0) &= \left(308, -232, \frac{3\pi}{4}, 0\right) \\ x_4(0) &= \left(0, -472, \frac{\pi}{2}, 0\right). \end{aligned} \tag{28}$$

In the numerical experiments, we use

$$\epsilon(x_i) \triangleq \min\{\psi_+(x_i), 16\} \tag{29}$$

to prevent $\mathbf{Q}_i$ from including too many constraints.

We performed two sets of numerical experiments, one with our external active-set algorithm and one without it—we call it a "native" use of the solver. For each set of experiments, we used various lengths of prediction horizon, $T = 7.5$, $T = 10$, and $T = 12.5$. Solution trajectories with $T = 10$ are shown in Fig. 22. We ran 50 iterations of MPC-guidance loop for each case, and the numerical results are summarized in Tables 4 and 5. In these tables, N_k^Q is the number of constraints in the set $\mathbf{Q}_i$ when our external active-set strategy terminates during solving kth FHOCP, t_k^C is the total CPU time for achieving an optimal solution at Step 2 of Algorithm IV.2, and $\%_t$ is the percentage of $\sum_k t_k^C$ with respect to the total allowed computation time for 50 iterations of MPC-based guidance algorithm $5.625 \times 50 = 281.25$. N_k^g, the total number of gradient evaluations at k-th MPC iteration, is defined as follows:

$$\begin{aligned} N_k^g = \sum_{i=0}^{i_T} |\mathbf{Q}_i| \times &\text{ number of gradient function} \\ &\text{calls during } i\text{th inner iteration for solving} \\ &k\text{th FHOCP} \end{aligned} \tag{30}$$

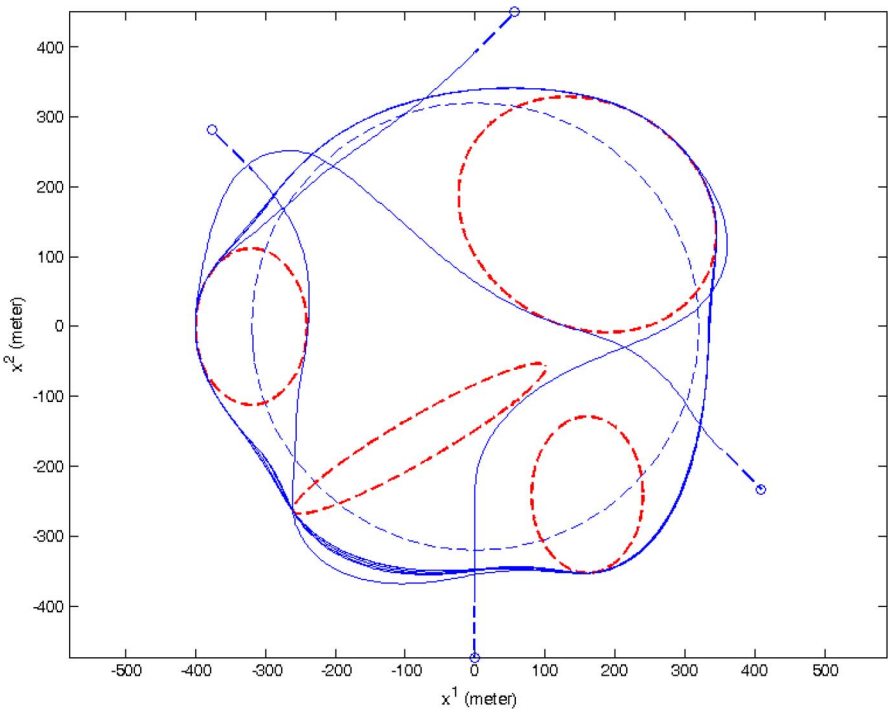

Fig. 22. ***Trajectories generated by Algorithm IV.2. The desired circular trajectory is in blue-dashed line, and no-flight zones in red-dashed line. The initial positions are marked as "o" and the blue-dashed straight lines in the beginning of trajectories denote the initial reference trajectories.***

where i_T is the value of the iteration index i at which Algorithm VI.1 is terminated by the termination tests incorporated in the optimization solver used. For "native" cases, $i_T = 1$ all the time.

As shown in Table 4, without our external active-set algorithm, none of computation results satisfied the real-time requirements. The values of $\max_k t_k^C$ show that it consumed 18 to 1000 times more computation time than the allowed computation time. However, with Algorithm IV.1, the total reduction in computation time was huge, and with $T = 7.5$ and $T = 10$ as shown in Table 5, it is feasible to apply the MPC-based guidance scheme to real-time trajectory generation.

V. CONCLUSION—ROBOTIC SENSOR WEB

As described in the introduction, one of the recent trends in the WSN research is to develop biologically inspired micromobile robots, integrate them with various MEMS sensors and wireless communication devices, and form an RSW. The demand for RSWs can be highlighted by the following real-world scenario.

Thanks to the constant video surveillance provided by tactical UAVs in the modern battlefields, it is relatively easy to remotely detect suspicious activities near an area of interest. For example, consider the village shown in Fig. 23. Suppose that a series of aerial surveillance photographs can be used to narrow down the targets to three buildings (marked A, B, and C), but the data are too coarse to choose one final target. It is a high-risk mission to send squads to all three buildings, since 1) they are spatially distributed and it makes the mission more difficult and dangerous, and 2) there is a possibility that one or more of these buildings may be traps—full of improvised explosive devices. It is risky to send a team of scouts or conventional remote-controlled ground robots, since all the insurgents in the building will relocate immediately once they detect scout activity. The mission objective is to discern the contents of these buildings and report it to the friendly force in the green zone.

TABLE 4 MPC-Based Guidance Using the Native SNOPT

T	N	$\max_k N_k^g$	$\max_k N_k^Q$	$\%_t$	$\max_k t_k^C$
7.5	24	555984	528	691.9	9.489e+02
10.0	32	45056	704	423.5	1.040e+02
12.5	40	2035440	880	3456.4	5.623e+03

TABLE 5 MPC-Based Guidance Using the External Active-Set Strategy With SNOPT

T	N	$\max_k N_k^g$	$\max_k N_k^Q$	$\%_t$	$\max_k t_k^C$
7.5	24	672	37	11.9	2.547
10.0	32	1026	67	29.3	4.483
12.5	40	1447	67	58.4	8.220

Fig. 23. ***A low-altitude aerial photo of a village (image from Google Earth mapping service).***

The example scenario described above shows the necessity of a wireless sensor network with stealth mobility. From the scenario, we can derive a set of required capabilities as follows.

1) *Accessing the interior of the building*: mobile sensing agents should be able to autonomously figure out how to gain entry to the interior of the building.
2) *Navigation through the interior of the building*: it is required for mobile sensing agents to be able to navigate inside the building in a stealthy manner to deploy wireless sensors and communication relays, track targets, report suspicious activities, etc.
3) *Communication to the base station*: mobile sensing agents should be able to report their sensor readings to the base station.

In 2008, MAST-CTA [42] funded by the United States Army Research Laboratory was initiated to encourage researchers to respond to new demands described above. The objective of MAST-CTA is to provide soldiers and disaster responders with better situational awareness in structured and unstructured dynamic environments using micro-RSWs. Under MAST-CTA, insect-like micro crawlers and flyers [23], [25]–[28] are being integrated with ultralight wireless inertial measurement units (IMUs) [22], which provide microrobotic sensor platforms for higher level algorithms like indoor mapping and localization [68], interagent cooperation [69], and communication-aware navigation [70]. They will be equipped with the state-of-art MEMS sensors such as a gas analyzer using microgas chromatograph [71], a microradiation detector [72], a hair-like actuator/sensor array [73], to name a few. Due to the small size of each robotic platform, a micro-RSW is expected to significantly improve the situational awareness in complex and dynamic environments into a level that cannot be reached by using conventional UAVs and UGVs.

An RSW, which is composed of stationary wireless sensors, robotic mobile agents, and human operators, is different from the traditional sensor networks that passively gather information: it is the network of heterogeneous components that are used to guide the actions of multiple decision makers operating in a dynamic environment. Accordingly, it can be seen as an extension of HSNs incorporating mobility and adaptivity. Current research in WSNs focuses only on one or two aspects, mostly because a comprehensive study of resource tradeoffs in WSNs is very challenging. On top of coupled computation, communication, and power, when mobility and heterogeneity, which are key properties of RSWs, are taken into account, the problem becomes even harder. Consequently, it is important to quantify high-confidence metrics for RSWs.

There exists a recent research about the metrics of WSN as a time-division multiple-access (TDMA) wireless mesh network [74]. It focuses on TDMA networks for ease of modeling and mesh networks for better path diversity and reliability. In many cases, deployed WSNs lack in-network data aggregation or processing, so it simply behaves as a self-organizing communication network (self-organizing in the sense that a WSN constructs its own routing topology and schedule). However, in RSWs, we need those regulations and adjustment by the system itself or by a human operator. The ongoing research concentrates on the scenario where there are fewer decision makers (e.g., controllers or human operators) in the network.

An RSW is meant to sense much more dynamic situations than conventional sensor networks, such as activities of people, and therefore high-bandwidth sensors, such as video cameras, will often be necessary. As well as the camera network localization algorithm described in the previous section, our group has worked on various aspects of distributed image processing over camera networks [75], [76]. These high-bandwidth sensors stress the traditional sensor network architectures in multiple ways. The most obvious one is that the power and bandwidth requirements of such nodes can be significantly higher. Data of widely different sizes may have to be transported over different protocols and this transport must be optimized for energy conservation and communication. Planning for tasks will require tools for the estimation of the resources needed and the optimization across multiple layers of the network.

It is obvious that technologies described in the previous sections are related to the capabilities of RSWs directly and indirectly. For example, the MPC-based trajectory planning algorithms can guide mobile sensing agents through narrow entrances and cluttered indoor environments. LochNess can provide a backbone of target-tracking algorithms over a mobile sensor network. Finally, the localization of camera network plays very critical role throughout the scenario. However, they are subject to new and stringent constraints on power, weight, and size, hence it is required to implement all the functions on less powerful processors. ■

REFERENCES

[1] C. Tomlin, G. J. Pappas, and S. Sastry, "Conflict resolution for air traffic management: A study in multi-agent hybrid systems," *IEEE Trans. Autom. Control*, vol. 43, no. 4, pp. 509–521, Apr. 1998.

[2] R. Fierro, A. Das, J. Spletzer, J. Esposito, V. Kumar, J. Ostrowski, G. Pappas, C. Taylor, Y. Hur, R. Alur, I. Lee, G. Grudic, and B. Southall, "A framework and architecture for multirobot coordination," *Int. J. Robot. Res.*, vol. 21, pp. 977–995, 2002.

[3] P. Stone and M. Veloso, "Multiagent systems: A survey from a machine learning perspective," *Autonom. Robots*, vol. 8, no. 3, pp. 345–383, 2000.

[4] M. A. Hsieh, A. Cowley, J. F. Keller, L. Chaimowicz, B. Grocholsky, V. Kumar, C. J. Talyor, Y. Endo, R. Arkin, B. Jung, D. Wolf, G. Sukhatme, and D. C. MacKenzie, "Adaptive teams of autonomous aerial and ground robots for situational awareness," *J. Field Robot.*, vol. 24, pp. 991–1014, 2007.

[5] M. Schwager, D. Rus, and J. J. Slotine, "Decentralized, adaptive coverage control for networked robot," *Int. J. Robot. Res.*, vol. 28, no. 3, pp. 357–375, 2009.

[6] D. Estrin, D. Culler, K. Pister, and G. Sukhatme, "Connecting the physical world with pervasive networks," *IEEE Pervasive Comput.*, vol. 1, no. 1, pp. 59–69, Jan. 2002.

[7] I. Akyidliz, W. Su, Y. Sankarasubramaniam, and E. Cayirci, "A survey on sensor networks," *IEEE Commun. Mag.*, vol. 40, no. 8, pp. 102–116, Aug. 2002.

[8] H. Gharavi and S. P. Kumar, Eds., "Sensor networks and applications," *Proc. IEEE*, vol. 91, no. 8, Aug. 2003, special issue.

[9] W. S. Jang and W. M. Healy, "Wireless sensor network performance metrics for building applications," *Energy Buildings*, vol. 42, no. 6, pp. 862–868, 2010.

[10] J. J. Evans, J. F. Janek, A. Gum, and B. L. Hunter, "Wireless sensor network design for flexible environmental monitoring," *J. Eng. Technol.*, vol. 25, no. 1, pp. 46–52, 2008.

[11] K. M. Yousef, J. N. Al-Karaki, and A. M. Shatnawi, "Intelligent traffic light flow control system using wireless sensors networks," *J. Inf. Sci. Eng.*, vol. 26, no. 3, pp. 753–768, 2010.

[12] F. Franceschini, M. Galetto, D. Maisano, and L. Mastrogiacomo, "A review of localization algorithms for distributed wireless sensor networks in manufacturing," *Int. J. Comput. Integr. Manuf.*, vol. 22, no. 7, pp. 698–716, 2009.

[13] C. Hsiao, R. Lee, I. Chou, C. Lin, and D. Huang, "A tele-emergent system for long-term ECG monitoring over wireless sensor network," *Biomed. Eng.—Appl. Basis Commun.*, vol. 19, no. 3, pp. 187–197, 2007.

[14] H. Yang and S.-H. Yang, "Indoor localization systems-tracking objects and personnel with sensors, wireless networks and RFID," *Meas. Control*, vol. 42, no. 1, pp. 18–23, 2009.

[15] X. Wang, S. Wang, and D. Bi, "Distributed visual-target-surveillance system in wireless sensor networks," *IEEE Trans. Syst. Man Cybern. B, Cybern.*, vol. 39, no. 5, pp. 1134–1146, Oct. 2009.

[16] P. Dutta, J. Hui, J. Jeong, S. Kim, C. Sharp, J. Taneja, G. Tolle, K. Whitehouse, and D. Culler, "Trio: Enabling sustainable and scalable outdoor wireless sensor network deployments," in *Proc. Int. Conf. Inf. Process. Sensor Netw., Special Track on Platform Tools and Design Methods for Network Embedded Sensors*, 2006, DOI: 10.1145/1127777.1127839.

[17] G. Werner-Allen, P. Swieskowski, and M. Welsh, *Motelab: A wireless sensor network testbed*, Los Angeles, CA, 2005, pp. 483–488.

[18] K. Sohrabi, J. Gao, V. Ailawadhi, and G. J. Pottie, "Protocols for self-organization of a wireless sensor network," *IEEE Personal Commun.*, vol. 7, no. 5, pp. 16–27, Oct. 2000.

[19] Y. Lin, B. Chen, and P. K. Varshney, "Decision fusion rules in multi-hop wireless sensor networks," *IEEE Trans. Aerosp. Electron. Syst.*, vol. 41, no. 2, pp. 475–488, Apr. 2005.

[20] A. Rahimi, B. Dunagan, and T. Darrell, "Simultaneous calibration and tracking with a network of non-overlapping sensors," in *Proc. Comput. Vis. Pattern Recognit.*, vol. 1, Jul. 2004, pp. 187–194.

[21] K. S. Pister and L. Doherty, "TSMP: Time synchronized mesh protocol," in *Proc. IASTED Int. Symp. Distrib. Sensor Netw.*, Orlando, FL, 2008, pp. 391–398.

[22] A. Mehta and K. Pister, "WARPWING: A complete open source control platform for miniature robots," in *Proc. IEEE/RSJ Int. Conf. Intell. Robots Syst.*, 2010, pp. 5169–5174.

[23] P. Birkmeyer, K. Peterson, and R. Fearing, "Dash: A dynamic 15 g hexapedal robot," in *Proc. IEEE Int. Conf. Intell. Robots Syst.*, 2009, pp. 2683–2689.

[24] A. Hoover, S. Burden, X.-Y. Fu, S. Sastry, and R. S. Fearing, "Bio-inspired design and dynamic maneuverability of a minimally actuated six-legged robot," in *Proc. IEEE Int. Conf. Biomed. Robot. Biomech.*, 2010, pp. 869–876.

[25] A. Hoover and R. Fearing, "Analysis of off-axis performance of compliant mechanisms with applications to mobile millirobots," in *Proc. IEEE Int. Conf. Intell. Robots Syst.*, 2009, pp. 2770–2776.

[26] J. Humbert, I. Chopra, R. Fearing, R. J. Full, R. J. Wood, and M. Dickinson, "Development of micromechanics for micro-autonomous systems (ARL-MAST CTA program)," in *Proc. SPIE*, 2009, vol. 7318, DOI:10.1117/12.820881.

[27] C. Li, A. M. Hoover, P. Birkmeyer, P. Umbanhowar, R. Fearing, and D. Goldman, "Systematic study of the performance of small robots on controlled laboratory substrates," in *Proc. SPIE Defense Security Sens. Conf.*, 2010, DOI: 10.1117/12.851047.

[28] E. R. Ulrich, D. J. Pines, and J. S. Humbert, "From falling to flying: The path to powered flight of a robotic samara nano air vehicle," *Bioinspirat. Biomimetics*, vol. 5, no. 4, 2010, DOI: 10.1088/1748-3182/5/4/045009.

[29] D. H. Shim, H. J. Kim, and S. Sastry, "Hierarchical control system synthesis for rotorcraft-based unmanned aerial vehicles," in *Proc. AIAA Guid. Navig. Control Conf.*, 2000, AIAA-2000-4057.

[30] D. H. Shim, "Hierarchical flight control system synthesis for rotorcraft-based unmanned aerial vehicles," Ph.D. dissertation, Dept. Mech. Eng., Univ. California Berkeley, CA, 2000.

[31] R. Vidal, O. Shakernia, H. J. Kim, H. Shim, and S. Sastry, "Multi-agent probabilistic pursuit-evasion games with unmanned ground and aerial vehicles," *IEEE Trans. Robot. Autom.*, vol. 18, no. 5, pp. 662–669, Oct. 2002.

[32] D. H. Shim, H. J. Kim, H. Chung, and S. Sastry, "Multi-functional autopilot design and experiments for rotorcraft-based unmanned aerial vehicles," in *Proc. 20th Digit. Avionics Syst. Conf.*, 2001, vol. 1, pp. 3C4/1–3C4/8.

[33] E. Shaw, H. Chung, S. Sastry, and J. K. Hedrick, "Unmanned helicopter formation flight experiment for the study of mesh stability," in *Cooperative Systems: Control and Optimization*, vol. 588, Lecture Notes in Economics and Mathematical Systems, D. Grundel, R. Murphey, P. Pardalos, and O. Prokopyev, Eds. Berlin, Germany: Springer-Verlag, 2007.

[34] H. J. Kim, D. H. Shim, and S. Sastry, "Flying robots: Modeling, control, and decision making," *Proc. IEEE Int. Conf. Robot. Autom.*, 2002, vol. 1, pp. 66–71.

[35] D. H. Shim, H. Chung, and S. Sastry, "Conflict-free navigation in unknown urban environments," *IEEE Robot. Autom. Soc. Mag.*, vol. 13, no. 3, pp. 27–33, Sep. 2006.

[36] D. H. Shim, H. J. Kim, and S. Sastry, "Decentralized nonlinear model predictive control of multiple flying robots in dynamic environments," in *Proc. IEEE Conf. Decision Control*, 2003, vol. 4, pp. 3621–3626.

[37] H. J. Kim and D. H. Shim, "A flight control system for aerial robots: Algorithms and experiments," *IFAC Control Eng. Practice*, vol. 11, no. 12, pp. 1389–1400, 2003.

[38] H. Chung, E. Polak, and S. S. Sastry, "An external active-set strategy for solving optimal control problems," *IEEE Trans. Autom. Control*, vol. 54, no. 5, pp. 1129–1133, May 2009.

[39] B. Sinopoli, C. Sharp, L. Schenato, S. Schaffert, and S. Sastry, "Distributed control applications within sensor networks," *Proc. IEEE*, vol. 91, no. 8, pp. 1235–1246, Aug. 2003.

[40] B. Sinopoli, L. Schenato, M. Franceschetti, K. Poolla, M. I. Jordan, and S. S. Sastry, "Kalman filtering with intermittent observations," *IEEE Trans. Autom. Control*, vol. 49, no. 9, pp. 1453–1464, Sep. 2004.

[41] S. Oh, L. Schenato, P. Chen, and S. Sastry, "Tracking and coordination of multiple agents using sensor networks: System design, algorithms and experiments," *Proc. IEEE*, vol. 95, no. 1, pp. 234–254, Jan. 2007.

[42] [Online]. Available: http://www.mast-cta-org

[43] J. Hill, M. Horton, R. Kling, and L. Krishnamurthy, "The platforms enabling wireless sensor networks," *Commun. ACM*, vol. 47, no. 6, pp. 41–46, 2004.

[44] R. Burkard and R. Çela, "Linear assignment problem and extensions," Karl-Franzens Univ. Graz, Graz, Austria, Tech. Rep. 127, 1998.

[45] S. Oh, S. Russell, and S. Sastry, "Markov chain Monte Carlo data association for multi-target tracking," *IEEE Trans. Autom. Control*, vol. 54, no. 3, pp. 481–497, Mar. 2009.

[46] P. W.-C. Chen, P. Ahammad, C. Boyer, S.-I. Huang, L. Lin, E. J. Lobaton, M. L. Meingast, S. Oh, S. Wang, P. Yan, A. Yang, C. Yeo, L.-C. Chang, D. Tygar, and S. S. Sastry, "CITRIC: A low-bandwidth wireless camera network platform," in *Proc. ACM/IEEE Int. Conf. Distrib. Smart Cameras*, Stanford, CA, Sep. 2008, DOI: 10.1109/ICDSC.2008.4635675.

[47] W. Mantzel, C. Hyeokho, and R. Baraniuk, "Distributed camera network localization," in *Proc. Asilomar Conf. Signals Syst. Comput.*, Nov. 2004, vol. 2, pp. 1381–1386.

[48] S. Funiak, C. Guestrin, M. Paskin, and R. Sukthankar, "Distributed localization of networked cameras," in *Proc. 5th Int. Conf. Inf. Process. Sensor Netw.*, Apr. 2006, pp. 34–42.

[49] R. Cucchiara, A. Prati, and R. Vezzani, "A system for automatic face obscuration for privacy purposes," *Pattern Recognit. Lett.*, vol. 27, no. 15, Nov. 2006, DOI: 10.1016/j.patrec.2006.02.018.

[50] J. Black, T. Ellis, and P. Rosin, "Multi view image surveillance and tracking," in *Proc. Workshop Motion Video Comput.*, 2002, pp. 169–174.

[51] L. Lee, R. Romano, and G. Stein, "Monitoring activities from multiple video streams: Establishing a common coordinate frame," *IEEE Trans. Pattern Anal. Mach. Intell.*, vol. 22, no. 8, pp. 758–767, Aug. 2000.

[52] M. Meingast, S. Oh, and S. Sastry, "Automatic camera network localization using object image tracks," in *Proc. IEEE Int. Conf. Comput. Vis.*, Rio de Janeiro, Brazil, Oct. 2007, DOI: 10.1109/ICCV.2007.4409214.

[53] M. Maróti, B. Kusý, G. Balogh, P. Völgyesi, A. Nádas, K. Molnár, S. Dóra, and A. Lédeczi, "Radio interferometric geolocation," in *Proc. ACM SenSys*, Nov. 2005, DOI: 10.1145/1098918.1098920.

[54] M. Meingast, M. Kushwaha, S. Oh, X. Koutsoukos, A. Ledeczi, and S. Sastry, "Fusion-based localization for a heterogeneous camera network," in *Proc. ACM/IEEE Int. Conf. Distrib. Smart Cameras*, Stanford, CA, Sep. 2008, DOI: 10.1109/ICDSC.2008.4635718.

[55] Y. Ma, S. Soatto, J. Kosecka, and S. Sastry, *An Invitation to 3-D Vision: From Images to Geometric Models*, ser. Interdisciplinary Applied Mathematics. New York: Springer-Verlag, Nov. 2003.

[56] EasyCal Calibration Toolbox. [Online]. Available: http://www.cis.upenn.edu/~kostas/tele-immersion/research/downloads/EasyCal/

[57] P. Dutta, M. Grimmer, A. Arora, S. Bibyk, and D. Culler, "Design of a wireless sensor network platform for detecting rare, random, and ephemeral events," in *Proc. 4th Int. Conf. Inf. Process. Sensor Netw., Special Track on Platform Tools and Design Methods for Network Embedded Sensors*, Apr. 2005, pp. 497–502.

[58] Y. K. Hwang and N. Ahuja, "Gross motion planning-a survey," *ACM Comput. Surv.*, vol. 24, no. 3, pp. 220–291, 1992.

[59] G. J. Sutton and R. R. Bitmead, "Performance and computational implementation of nonlinear model predictive control on a submarine," in *Nonlinear Model Predictive Control*, vol. 26, F. Allgoöwer and A. Zheng, Eds. New York: Birkhäuser, 2000, vol. 26, pp. 461–471.

[60] D. H. Shim and S. Sastry, "A situation-aware flight control system design using real-time model predictive control for unmanned autonomous helicopters," in *AIAA Guid. Navig. Control Conf.*, 2006, AIAA-2006-6101.

[61] K. Holmström, A. O. Göran, and M. M. Edvall, *User's Guide for TOMLAB*, Tomlab Optimization Inc., Dec. 2006.

[62] W. Murray, P. E. Gill, and M. A. Saunders, "SNOPT: An SQP algorithm for large-scale constrained optimization," *SIAM J. Optim.*, vol. 12, pp. 979–1006, 2002.

[63] P. E. Gill, W. Murray, M. A. Saunders, and M. H. Wright, "User's guide for NPSOL 5.0: A fortran package for nonlinear programming," Syst. Optim. Lab., Dept. Operat. Res., Stanford Univ., Stanford, CA, Tech. Rep. SOL 86-2, 1998.

[64] K. Schittkowski, "On the convergence of a sequential quadratic programming method with an augmented Lagrangian line search function," Syst. Optim. Lab., Stanford Univ., Stanford, CA, Tech. Rep., 1982.

[65] E. Polak, *Optimization: Algorithms and Consistent Approximations*, ser. Applied Mathematical Sciences. New York: Springer-Verlag, 1997, vol. 124.

[66] I. M. Mitchell, A. M. Bayen, and C. J. Tomlin, "A time-dependent Hamilton-Jacobi formulation of reachable sets for continuous dynamic games," *IEEE Trans. Autom. Control*, vol. 50, no. 7, pp. 947–957, Jul. 2005.

[67] Y. Kang and J. K. Hedrick, "Linear tracking for a fixed-wing UAV using nonlinear model predictive control," *IEEE Trans. Control Syst. Technol.*, vol. 17, no. 5, pp. 1202–1210, Sep. 2009.

[68] R. He, A. Bachrach, M. Achtelik, A. Geramifard, D. Gurdan, S. Prentice, J. Stumpf, and N. Roy, "On the design and use of a micro air vehicle to track and avoid adversaries," *Int. J. Robot. Res.*, vol. 29, no. 5, pp. 529–546, 2010.

[69] N. Michael, J. Fink, and V. Kumar, "Cooperative manipulation and transportation with aerial robots," *Autonom. Robots*, vol. 30, no. 1, pp. 73–86, Jan. 2011.

[70] Y. Mostofi, "Decentralized communication-aware motion planning in mobile networks: An information-gain approach," *J. Intell. Robot. Syst.*, vol. 56, pp. 233–256, 2009.

[71] S.-J. Kim, S. Reidy, B. Block, K. Wise, E. Zellers, and K. Kurabayashi, "A low power, high-speed miniaturized thermal modulator for comprehensive 2D gas chromatography," in *Proc. IEEE Int. Conf. Microelectromech. Syst.*, Piscataway, NJ, 2010, pp. 124–127.

[72] C. K. Eun and Y. B. Gianchandani, "A microfabricated steel and glass radiation detector with inherent wireless signaling," *J. Micromech. Microeng.*, vol. 21, 015003, 2011.

[73] M. Sadeghi, H. Kim, and K. Najafi, "Electrostatically driven micro-hydraulic actuator arrays," in *Proc. IEEE Int. Conf. Microelectromech. Syst.*, 2010, pp. 15–18.

[74] P. W. Chen, "Wireless sensor network metrics for real-time systems," Ph.D. dissertation, Electr. Eng. Comput. Sci. Dept., Univ. California Berkeley, Berkeley, CA, May 2009.

[75] A. Yang, S. Maji, K. Hong, P. Yan, and S. Sastry, "Distributed compression and fusion of nonnegative sparse signals for multiple-view object recognition," in *Proc. Int. Conf. Inf. Fusion*, 2009, pp. 1867–1874.

[76] A. Yang, J. Wright, S. Sastry, and Y. Ma, "Unsupervised segmentation of natural images via lossy data compression," *Comput. Vis. Image Understand.*, vol. 110, no. 2, pp. 212–225, 2008.

ABOUT THE AUTHORS

Hoam Chung (Member, IEEE) received the B.A. and M.S. degrees in precision mechanical engineering from Hanyang University, Seoul, Korea, in 1997 and 1999, respectively, and the Ph.D. degree in mechanical engineering from the University of California Berkeley, Berkeley, in May 2006.

He has worked in the Intelligent Machines and Robotics Laboratory at the University of California Berkeley as a Postdoctoral Researcher and a Research Scientist from 2006 to 2009. He has led Autonomous Systems Group in the lab from 2007 to 2009, and has participated in various projects including ARO MURI SWARMS and MAST-CTA. He joined the Faculty of Engineering at Monash University, Clayton, Vic., Australia, in 2010, and is now a Lecturer in the Department of Mechanical and Aerospace Engineering. His research interests include receding horizon control (RHC) theory and application, autonomous miniature flyers, semi-infinite optimization problems, real-time system design and implementation, and autonomous unmanned systems [unmanned aerial vehicles (UAVs), unmanned ground vehicles (UGVs), and unmanned undersea vehicles (UUVs)].

Songhwai Oh (Member, IEEE) received the B.S. (with highest honors), M.S., and Ph.D. degrees in electrical engineering and computer sciences from the University of California Berkeley, Berkeley, in 1995, 2003, and 2006, respectively.

Currently, he is an Assistant Professor in the School of Electrical Engineering and Computer Science, Seoul National University, Seoul, Korea. His research interests include cyber-physical systems, wireless sensor networks, robotics, estimation and control of stochastic systems, multimodal sensor fusion, and machine learning. Before his Ph.D. studies, he worked as a Senior Software Engineer at Synopsys, Inc. and a Microprocessor Design Engineer at Intel Corporation. In 2007, he was a Postdoctoral Researcher at the Electrical Engineering and Computer Sciences Department, University of California Berkeley, Berkeley. From 2007 to 2009, he was an Assistant Professor of Electrical Engineering and Computer Science in the School of Engineering, University of California Merced, Merced.

David Hyunchul Shim (Member, IEEE) received the B.S. and M.S. degrees in mechanical design and production engineering from Seoul National University, Seoul, Korea, in 1991 and 1993, respectively, and the Ph.D. degree in mechanical engineering from the University of California Berkeley, Berkeley, in 2000.

From 1993 to 1994, he was with Hyundai Motor Company, Korea, as Transmission Design Engineer. From 2001 to 2005, he was with Maxtor Corporation, Milpitas, CA as Staff Servo Engineer specialized in advanced servo control systems for hard disk drives. From 2005 to 2007, he was with the University of California Berkeley as Principal Engineer, in charge of Berkeley Aerobot Team, working on advanced unmanned aerial vehicles (UAVs) programs such as DARPA SEC and UCAR. In 2007, he joined the Department of Aerospace Engineering, Korea Advanced Institute of Science and Technology (KAIST), Daejon, Korea, as an Assistant Professor. He is now an Associate Professor working on various research projects on UAVs in the area of flight dynamics and control, multiagent coordination, and unmanned ground systems.

S. Shankar Sastry (Fellow, IEEE) received the Ph.D. degree in electrical engineering and computer science from the University of California Berkeley, Berkeley, in 1981.

He is currently the Dean of the College of Engineering. He was the Chairman, Department of Electrical Engineering and Computer Sciences, University of California Berkeley, from 2001 to July 2004. Until August 2007, he was the Director of the Center for Information Technology Research in the Interest of Society (CITRIS), University of California Berkeley. He served as Director of the Information Technology Office at DARPA from 1999 to 2001. From 1996 to 1999, he was the Director of the Electronics Research Laboratory at Berkeley, an organized research unit on the Berkeley campus conducting research in computer sciences and all aspects of electrical engineering. He has supervised over 50 doctoral students to completion and over 50 M.S. students. His students now occupy leadership roles in several locations such as Dean of Engineering at the California Institute of Technology (Caltech), Pasadena, Director of Information Systems Laboratory, Stanford University, Stanford, CA, Army Research Office, and on the faculties of every major university in the United States and abroad.

Dr. Sastry is the NEC Distinguished Professor of EECS, Bioengineering, and Mechanical Engineering. He was elected into the National Academy of Engineering in 2001 "for pioneering contributions to the design of hybrid and embedded systems." He was also elected to the American Academy of Arts and Sciences in 2004. He received the President of India Gold Medal in 1977, the IBM Faculty Development award for 1983–1985, the National Science Foundation (NSF) Presidential Young Investigator Award in 1985, and the Eckman Award of the of the American Automatic Control Council in 1990, an M.A. (*honoris causa*) from Harvard University in 1994, the distinguished Alumnus Award of the Indian Institute of Technology in 1999, and the David Marr prize for the best paper at the International Conference in Computer Vision in 1999 and the Ragazzini Award of the American Control Council in 2005.